Supplementary Material for

Structure and conformation of photosynthetic pigments and related compounds. 15. Conformational analysis of chlorophyll derivatives – Implications for Hydroporphyrins *in vivo*.

Dáire Gibbons,[a] Keith J. Flanagan,[a] Léa Pounot,[a] and Mathias O. Senge[a,*]

[a] School of Chemistry, SFI Tetrapyrrole Laboratory, Trinity Biomedical Sciences Institute, Trinity College Dublin, The University of Dublin, 152-160 Pearse Street, Dublin 2, Ireland.

The supplementary material is arranged in the same sequence as the relevant sections of the main manuscript.

Table of Contents:

1. Description of Test Case NSD Analyses

1.1 NSD Analysis of free base 5,10,15,20-tetraphenylporphyrin (TPP) crystal structures

	CCDC	Color	Solvent	Ref.
6a	JIVRAH		Benzaldehyde	25a
6b	SEMNIH		1,3-dimethylbenzene	25b
6c	SEMNIH01		1,3-dimethylbenzene	25c
6d	TPHPOR01		No solvent	25d
6e	TPHPOR04		No solvent	25f
6f	TPHPOR11		No solvent	25g
6g	TPHPOR12		No solvent	25h
6h	TPHPOR13		No solvent	25i
6i	TPHPOR14		No solvent	25j
6j	XAGLOG		Anthracene	25k
6k	XAGMAT		Pyrene	25l

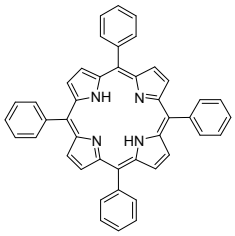

Figure S1 TPP structures (**6**) from CCDC and table containing CCDC reference, the color corresponding to the NSD analysis, and solvent within the unit cell.

The TPP compounds[25] with the highest D_{oop}, (TPHPOR01-TPHPOR14), contain no solvent within its unit cell (0.225–0.269 Å). The *wav*(x) of these TPPs range from 0.207–0.253 Å and the *wav*(y) range is from 0.088–0.115 Å, (absolute values are given). For the structure of JIVRAH, a benzaldehyde solvent yields a D_{oop} value of 0.015 Å and the *wav*(x) and *wav*(y) values are -0.012 and 0.009 Å, respectively. These distortions are due to a predominant intermolecular hydrogen bonding network between the aldehyde and the β-hydrogen atoms of the nearest porphyrin molecule. Additionally, there are several hydrogen···π-interactions between the aldehyde and the phenyl rings of the porphyrin. This results in the benzaldehyde solvent being held above and below the porphyrin plane, staggering the porphyrin stacking and increasing its planarity. The structures of SEMNIH and SEMNIH01 show a marked decrease of almost 0.100 Å to the D_{oop} compared to the non-solvated structures of TPP. This can be rationalized by the 1,3-dimethylbenzene solvent present in the unit cells. This solvent interacts with an α-carbon of one TPP and a phenyl ring of a different TPP molecule. Additionally, the phenyl rings interact *via* short hydrogen contacts in a head-to-head style packing system. This head-on interaction, as well as the solvent interactions, give rise to a slightly staggered head-on packing system. SEMNIH has distortions of 0.039 Å and -0.003 Å in the *wav*(x) and *wav*(y) modes, respectively, whereas distortions of -0.001 Å and -0.037 Å are seen in these modes. The introduction of a large aromatic solvent, as seen in XAGLOG (anthracene) and XAGMAT (pyrene), within the crystal structure yields similar D_{oop} values (0.218 Å and 0.258 Å, respectively) to the non-solvated TPPs. However, when looking at the specific distortion modes, a clear shift of preference from the *wav*(x) to the *wav*(y) mode is seen by the inclusion of a large aromatic solvent. These aromatic solvents give *wav*(y) distortions of 0.176 Å in XAGLOG and 0.215 Å in XAGMAT and a *wav*(x) distortion of 0.129 Å in and 0.143 Å, respectively.

The *oop* distortions give a good pictorial overview of how solvent effects influence the tetrapyrrole's conformation. However, a complete overview of the 3D configuration in TPPs is not obtained without discussing the in-plane (*ip*) distortion as well. The largest *ip* contribution to the TPP structure comes from the *bre* mode. This mode measures the total compression and stretching in the 24-atom tetrapyrrole ring. The TPP series contains a range of *bre* NSD values between 0.158–0.226 Å and from these values, there does not seem to be a trend associated with the presence of a solvent in the unit cell. Other smaller contributions in this free base TPP series include *m-str* and *N-str* with a range of 0.04–0.056 Å in *m-str* and -0.042 to 0.053 Å in *N-str* (absolute values are given). The smallest contribution seen is given by *rot*. There is little to no *trn*(x) and *trn*(y) distortion in these TPP compounds. Therefore, this analysis proves that the small solvents can influence the macrocycle conformation due to intermolecular interactions resulting in a more planar *oop* conformation. The D_{oop} range is narrow in the TPPs with either no solvent or a large solvent incorporated into the 3D structure. In these types of TPPs, a clear preference of *wav*(x) over *wav*(y) distortion is clearly shown. However, in the *ip* distortion, no solvent effects are visible and the NSD values appear to be generally low, which is characteristic for TPP.

1.2 NSD Analysis of free base 2,3,7,8,12,13,17,18-octaethylporphyrin (OEP) crystal structures

When the free base 2,3,7,8,12,13,17,18-octaethylporphyrin (OEP, **7**) species were being studied, only two structures were taken from the CSD.[26] These compounds have CCDC codes OETPOR10 (**7a**) and OKOQUA (**7b**). A third compound, VEPHUV was disregarded due to the large, bulky fullerene solvent. **7a** contains no solvent in its crystal structure and it has a slightly staggered end-on packing system *via* the β-ethyl groups. The structure of compound **7b** contains a tetracyanoquinodimethane solvent within its unit cell. The solvent in **7b** occupies a cavity in between two porphyrins. There is evidence of π-stacking between the porphyrin and the conjugated solvent. This plays a small role in changing the packing system as it increases the mean plane distance of each porphyrin molecule from each other. Therefore, this creates a cavity for the solvent to occupy itself. However, the solvent appears not to have any significant impact on the NSD. The two OEP structures both have very similar NSD profiles except the *wav*(x) mode of distortion, which is approximately three times larger in **7a** (-0.063 Å) than **7b** (-0.018 Å) and the OEPs have very similar *wav*(y) distortions (0.090 Å in **7a** and -0.092 Å in **7b**). Similar to the TPPs previously discussed, most of their *oop* information is given by *wav*(x) and *wav*(y). They have little contribution from the *sad*, *ruf*, and *dom* distortions in both OEP crystal structures (Fig. S2).

The OEPs *ip* distortion, however, shows a different image. The NSDs indicate that there is very little contribution from *trn*(x), *trn*(y) and *rot*. The main contribution for the two OEPs comes from the *bre ip* distortion mode with values of approximately 0.220 Å. The most interesting distortion for these OEPs is *m-str*. For the conjugated derivative **7b**, the *m-str* deviation from the plane is greater than the non-solvated crystal structure by a factor of over 100 with values of 0.233 Å (**7b**) compared to 0.002 Å (**7a**). This *m-str* distortion is evident that steric bulk interactions are present involving the meso-carbon of one porphyrin and the β-substituents of another, giving rise to the large *m-str* distortion that contributes to the overall 3D configuration.

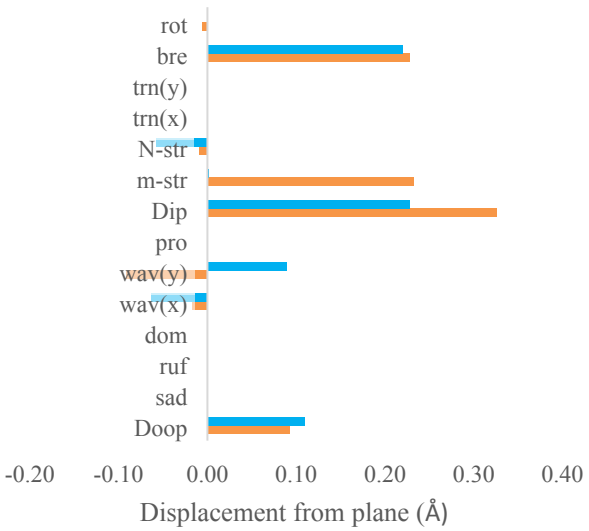

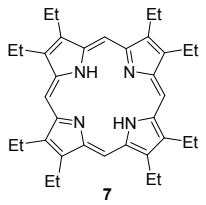

	CCDC	Color	Solvent	Ref.
7a	OETPOR10		No solvent	26a
7b	OKOQUA		Tetracyanoquinodimethane	26b

Figure S2 OEP series and NSD analysis of the X-ray crystallographic structures observed in the OEP compounds listed in the table. Table contains their CCDC reference codes, color corresponding to the NSD analysis, and solvent in the respective unit cell.

1.3 Free base tetraphenylporphyrins with an increasing number of β-substituted ethyl groups (XEtTPP)

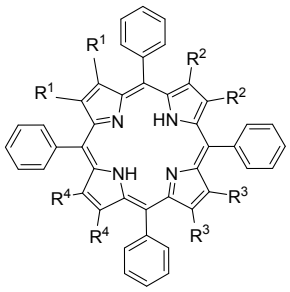

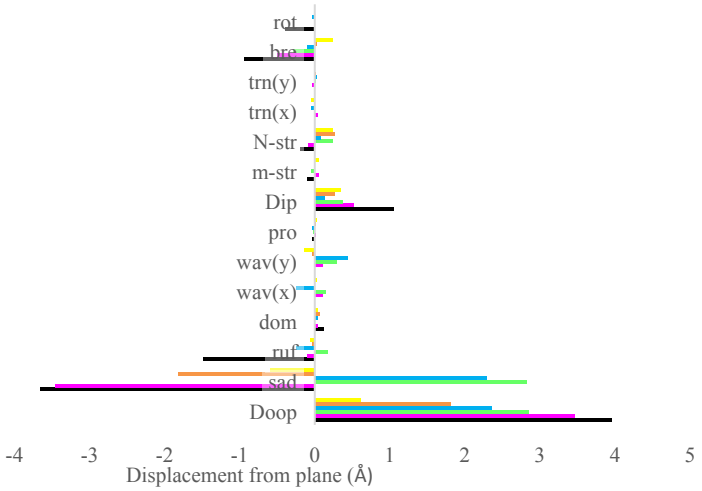

	CCDC	Color	R^1	R^2	R^3	R^4	Solvent	Ref.
8	TATPOT01		Et	H	H	H	No solvent	27b
9	TATPUZ01		Et	H	Et	H	DCM	27b
10	TATQAG01		Et	Et	H	H	MeOH	27b
11	TATQEK01		Et	Et	Et	H	DCM	27b
12	SATQOU		Et	Et	Et	Et	EtOH	27c
12a	QAWFIE		Et	Et	Et	Et	DCM	27c

Figure S3 XEtTPP series and NSD analysis of the X-ray crystallographic structures observed in the XETPP compounds listed in the table. Table contains their CCDC reference codes, color corresponding to the NSD analysis, specific functional groups (R^1-R^4), and solvent in the respective unit cell.

The compounds under study are shown in Fig. S3. The D_{ip} follows the reoccurring trend seen in the D_{oop} with a few exceptions. Compound **10** has a lower D_{ip} than **6h,** whose *ip* distortion is slightly lower than **9**. Porphyrin **8**, being more distorted in the D_{ip} than **9**, is not as distorted as **11**.[27b] The next most distorted structure in this series is **12**. Moving onto **12a** involves a twofold increase in D_{ip} distortion. As discussed in the TPP section, the D_{ip} distortion area is as significant as the D_{oop}.[27b,c]
However, in comparison to the highly substituted porphyrin like **12a**, the D_{ip} modes, while still significant, appear to have less impact on the overall conformation. While **12a** contains the largest *m-str* distortion, the trend, seen in the D_{oop} and the *sad* mode, is absent in this *ip* mode. Structures **9** and **10** contain almost no *m-str* distortion, while **6h**, **8**, **11** and **12** contain similar and significant *m-str* conformations that are roughly half the distortion observed in **12a**. There is no trend observed in the *N-str* mode as the structure with the largest distortion is **9**. This is closely followed by **8** and **11**. The trend discussed in the *m-str* distortion is very similar to the *bre* distortion. Compounds **9** and **10** have the lowest *bre* conformations, whereas **1** and **8** have a slightly higher distortion than **9** and **10** in this mode and the structure with the next highest *bre* conformation is **11**. One of the highly substituted porphyrins, **12**, has almost double the *bre* distortion seen in **11**. The contribution to this mode is then approximately doubled to get to the *bre* conformation in **12a**. For all the listed compounds, the contributions of *trn*(x) and *trn*(y) modes have very little input in the *ip* distortion. Similarly, the *rot* appears negligible with only compound **12a** showing any significant contribution.

1.4 Free base chlorins with additional ethyl groups on the β positions (XEtTPC)

The NSD analysis for this group of compounds is shown in Fig. S4. Compound **13** contains the smallest D_{oop}, **14** has the second largest D_{oop} and the most interesting observation in the D_{oop} is that **14** (DEtTPC) has a larger D_{oop} than **15** (cis-TEtTPC). Chlorin **16** contains the largest D_{oop} in the free base chlorins.[28] The D_{oop} and *sad* distortion increase when the number of β-ethyl groups increases with the exception of **14** and **15**. For the *ruf* distortion, a new trend is seen where **15** has a larger *ruf* than **16**. The structure of **16** contains the second largest *ruf* conformation, which is then larger than **14**. The DEtTPC **13** is the structure with the smallest *sad* and *ruf* distortion. In the *dom* distortion mode, the structures with the most *dom* distortions are the structures with four ethyl groups on the periphery of the chlorin heterocycle (**15**). The DEtTPCs, **13** and **14**, have a smaller *dom* distortion than **15** and **16**. The *wav*(x) distortion mode follows the same trend as the D_{oop} and *sad* as **16** has the largest distortion. Compound **14** has the second largest distortion followed by **15** with the second smallest distortion and **13** has the smallest *wav*(x) distortion. The *wav*(y) mode follows a similar trend to the *dom* mode in these chlorins as **13** and **14** have the two smallest *wav*(y) conformations (**14** is the smallest) and **15** and **16** contain the highest distortions in this mode (**16** is the highest). In the *pro* distortion mode, all contributions are negligible bar that of **15**. As seen in the porphyrin section, the higher number of ethyl groups attached to the β-carbons of the chlorin, the more non-planar the macrocycle becomes. However, there is also a reduced bond placement trend observed in this section. This trend suggests that the further away the ethyl groups are from the reduced pyrrole, the more D_{oop} present in the structure.
Contrary to the *oop* modes of distortion in this series, the structures with the lowest number of ethyl groups on the β-positions have the highest D_{ip}. This is shown by **13** and **14** having the highest D_{ip} with **15** and **16** having the lowest D_{ip}. The second DEtTPC, **14**, contains the lowest *m-str* distortion. The structure with the second lowest conformation in this mode is **16** whereas **13** is slightly higher in terms of *m-str* distortion. However, the first cis-TEtTPC, **15,** contains the highest *m-str* distortion as it is approximately three times more distorted than **13**. The free base chlorin with the lowest *N-str* distortion is **15**. An addition of 0.020 Å to the *N-str* distortion yields the *N-str* distortion of **16** but **13** is slightly more distorted in this mode. Through the almost threefold increase of **13**'s *N-str* distortion, **14**'s *N-str* distortion is achieved. In the *bre* mode, **14** and **15** are approximately three times lower than the *bre* distortion in **16** and yet again, **13** has a higher *ip* distortion as it is

almost 0.100 Å higher in its *bre* contribution than **16**. The *trn*(x), *trn*(y), and *rot* distortion modes appear to have no significant contribution to the 3D structures of these chlorins. Overall, the decrease in steric bulk increases the *ip* distortion and there is no reduced bond placement effect on the *ip* modes.

	CCDC	Color	R^1	R^2	R^3	R^4	Solvent	Ref.
13	GELGUZ		Et	H	H	H	No solvent	28
14	GELJEM		H	Et	H	H	MeOH	28
15	GELQAP		H	H	Et	Et	DCM/MeOH	28
16	GELHAG		H	Et	Et	H	DCM	28

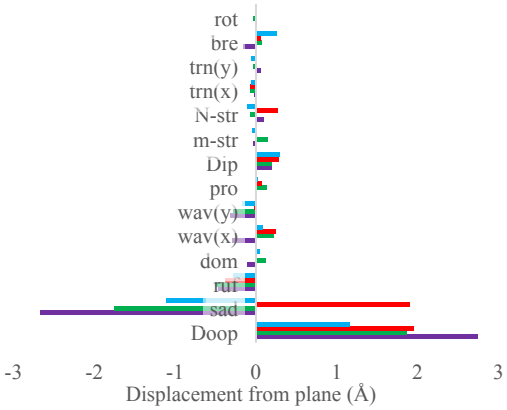

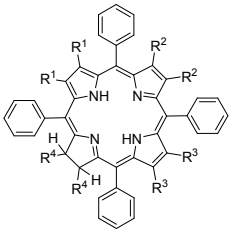

Figure S4 XEtTPC series and NSD analysis of the X-ray crystallographic structures observed in the XETPC compounds listed in the table. Table contains their CCDC reference codes, the color corresponding to the NSD analysis, specific functional groups (R^1-R^4), and solvent in their unit cell.

1.4.1 Impact of reduction on the distortion in the free base compounds in TEtTPCs versus TEtTPPs:

The next set of compounds that will be discussed in terms of the impact of reduction on the NSD is the cis-TETPP, **10**, cis-TETPCs, **15** (ethyl groups on the β-position of the chlorin pyrrole) and **16** (ethyl groups are adjacent to the chlorin pyrrole). The D_{oop} is larger in **16** than **10** and the D_{oop} of **10** is 0.487 Å higher than **15**. This same trend is also seen in the *sad* and *wav*(x) distortion modes. In the *ruf* distortion, **15** has the largest deviation followed by **16** and then **10**. This trend is also seen in the *dom* distortion mode. In the *wav*(y), the largest contribution in **10** is followed by **16** and then **15**. In the last mode of *oop* distortion (*pro*), **15** and **16** show similar large contributions and there is a moderate decrease in distortion in the structure of **10**. There is no clear trend between these structures, however, the chlorin that has the furthest distance between the ethyl groups and the reduced pyrrole has the largest *oop* distortion.

The structure of **16** shows the largest D_{ip} distortion closely followed by **15** with compound **10** showing a moderate decrease in D_{ip}. In the *m-str*, the largest contribution is from **15** with a substantial decrease seen in both **16** and **10**. Cis-TEtTPC, **16**, has the largest *N-str* distortion being marginally larger than **10** and **15**. In the *trn*(x) mode of distortion, **15** has the highest contribution to the *ip* distortion and **10** is the second highest with **16** being the smallest contribution. The opposite is observed for the *trn*(y) with **16** having the largest contribution and both **15** and **10** displaying a minor reduction in distortion. **16** has the highest *bre* distortion followed by **10** then **15.** In the *rot* mode, **10** has the exact same distortion as **15.** This distortion is more than three times greater than the *rot* distortion seen in **16**. The cis-TETPCs have a higher overall *ip* distortion than the cis-TETPPs.

1.5 Zinc(II) complexes

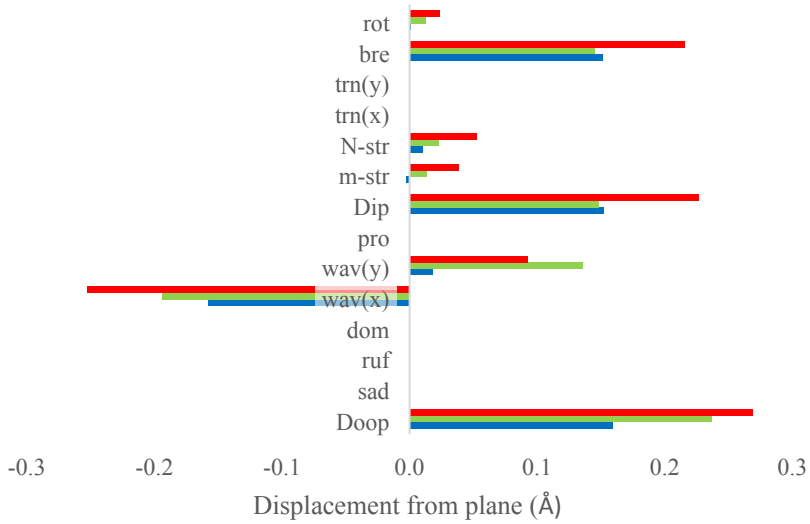

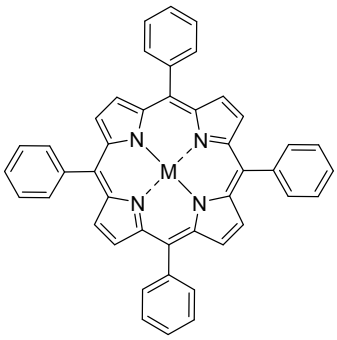

	CCDC	Color	M	Ref.
6h	TPHPOR13		2H	25i
Zn6a	ZZZTAY02		Zn(II)	30
Zn6b	ZZZTAY03		Zn(II)	32

Figure S5 Zn(II)TPP series and NSD analysis of the X-ray crystallographic structures observed in the Zn(II)TPP compounds listed in the table. Table contains their CCDC reference codes, color corresponding to the NSD analysis, and the metal(II) center.

Zn(II)TPP: The Zn(II)TPPs[30,32] (Fig. S5) have a slightly smaller deviation from the 24-atom mean plane than the free base TPPs as shown by their D_{oop}s. Zn(II)TPPs **Zn6a** and **Zn6b**, as with the free base TPP's, have little to no contributions to the D_{oop} with the only significant contributions found in the *wav*(x) and *wav*(y). There is a small decrease in the *wav*(x) distortion mode compared to the TTP samples above and similar contributions found in the *wav*(y). However, in the *ip* modes of distortion, there is a clear decrease in the distortion found in D_{ip}, *m-str*, *N-str*, *bre*, and *rot* modes compared to the TPP's. No differences are observed for the *trn*(x) and *trn*(y). While the Zn(II)'s *oop* distortion is similar yet slightly less than that of the free base, there is a more notable difference in the *ip* distortion. While the crystal packing plays a role in the difference observed in distortion between the two sets of TPPs, the contraction of the Zn metal in the core seems to be the main difference.

Zn(II)OEP: This next section comprises a discussion of the NSD results observed in the Zn(II)OEPs (Fig. S6)[26b,31a] as well as comparing these results with the free base OEPs. The first thing to note is that the inclusion of solvent appears to drastically increase the D_{oop} values as seen with **Zn7b** with significant contributions seen in the *sad* mode for **Zn7b**. However, looking at the solvent free structures of **7a** and **Zn7a**, a slightly different trend is observed. In general, there is a moderate increase in D_{oop} values which is a result of a significant increase in the *wav*(x) distortion mode. However, this appears to be coupled with a reduction in values of the *wav*(y) due to the inclusion of a Zn(II) metal center into the core of the porphyrin. In the *ip* distortion modes, there is a decrease in values as a result of Zn(II) inclusion to the core of the macrocycle. This appears to be independent of solvent effects as **Zn7a** and **Zn7b** have very similar values. The main distortion mode that affects this decrease is seen in the *bre* distortion mode. It represents the exact trend seen in the D_{ip} and the remaining *ip* distortion modes appear to have little to no effect. The only exception to this is seen in the *m-str* contribution of **7b**.

Overall, with the exception of **Zn7a**, there seems to be an inverse relationship between the D_{oop} and the D_{ip} in the free base and Zn(II)OEPs. The free base OEPs have a smaller D_{oop} than the Zn(II)OEPs but they have a larger D_{ip} than the Zn(II) compounds. Therefore, the inclusion of a Zn(II) metal into the OEP core causes the macrocycle in this molecule to become more non-planar while reducing the *ip* distortion.

Zn(II)XEtTPP: When looking at the effect Zn(II) metal insertion has on more highly substituted systems (Fig. S7) Zn(II)XEtTPPs (**Zn8**–**Zn12**)[27b,31b] were compared to their free base counterparts (**8**, **9**, **11** and **12**). Taking the DEtTPP (**8** and **Zn8**), it is quite evident that a larger increase in D_{oop} is observed as a result of Zn(II) inclusion to the porphyrin core. This increase is the result of a general increase to all the *oop* distortion modes bar *pro*. The largest increases are seen in the *sad* and *ruf* distortion modes with the *dom* and *wav*(x) showing a more temperate increase in distortion. The increase in *dom* distortion is due to the presence of an axial ligand. The *wav*(y) only shows a minor increase in distortion. When looking at the *ip* distortion modes, it is clear that the inverse happens here in comparison to the *oop*. There is a clear reduction in values in the D_{ip}, *m-str*, *N-str*, *trn*(x), and *bre* distortion modes with the most significant deviations observed in the *N-str* and *bre* distortion modes. The increases of observed *trn*(y) and *rot* distortion modes are rather quite negligible.

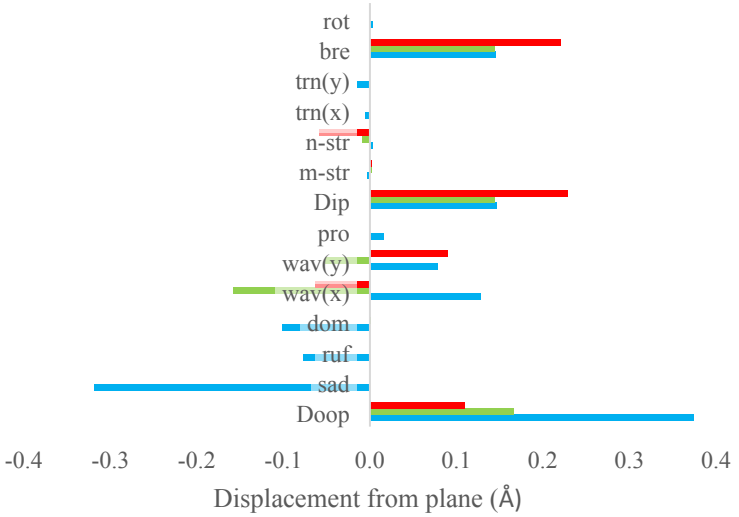

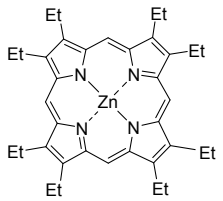

	CCDC	Color	Solvent	Ref.
7a	OETPOR10		No solvent	26a
Zn7a	ALOKOB		No solvent	31a
Zn7b	OKOREL		Tetracyanoquinodimethane	26b

Figure S6 Zn(II)OEP series and NSD analysis of the X-ray crystallographic structures observed in the Zn(II)OEP compounds listed in the table. Table contains their CCDC reference codes, color corresponding to the NSD analysis, and solvent in the respective unit cell.

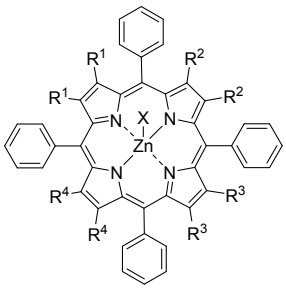

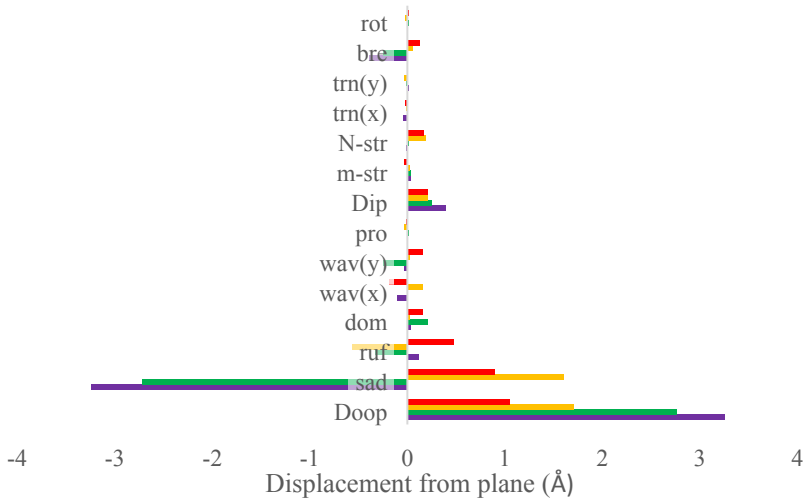

	CCDC	Color	R^1	R^2	R^3	R^4	X	Ref.
Zn8	RUTNEZ		Et	H	H	H	toluene	27b
Zn9	RUTQAY		Et	H	Et	H	Benzene	27b
Zn11	RUTRAZ		Et	Et	Et	H	-	27b
Zn12[a]	JICNIS		Et	Et	Et	Et	MeOH	31b

Figure S7 Zn(II)XEtTPP series and NSD analysis of the X-ray crystallographic structures observed in the Zn(II)XEtTPP compounds listed in the table. Table contains their CCDC reference codes, color corresponding to the NSD analysis, specific functional groups (R^1-R^4), and axial ligand. [a]Contains MeOH solvent.

Moving to the tTEtTPP (**9** and **Zn9**), the difference between the D_{oop} is rather less pronounced than in the DETPP section above. A minor decrease is observed in the D_{oop} as a result of the Zn(II) metal insertion to the porphyrin core. This is a result of a decrease in *sad* character coupled with an increase in *ruf* and *wav*(x) character of the porphyrin macrocycle. The axial ligand does not seem to play a huge role here compared to the DEtTPPs as the *dom* distortion has decreased due to the Zn(II) metal being inserted and the axial ligand being attached. In the *ip* distortion modes, there is only a moderate decrease in the D_{ip} as a result of Zn(II) metal insertion into the core of the porphyrin. This insertion results in a decrease in the *N-str* character of the porphyrin.

Looking at the HEtTPP porphyrin (**11** and **Zn11**), as with trans-TEtTPP above, there is only a small decrease in the D_{oop}. This stems from a moderate decrease in the *sad* and *wav*(x) distortion modes coupled with an increase of *ruf* and *dom* character of these porphyrins. Similarly, there is a moderate decrease in the D_{ip} distortions due to a significant decrease in the *N-str* distortion mode.

For the OEtTPP (**12** and **Zn12**) there is a moderate decrease in the D_{oop} due to a decrease in the *sad* and *wav*(y) distortion modes as a Zn(II) metal center is inserted into the parent porphyrin. The rest of the *oop* distortions modes have little to no difference. The same result is seen here that was seen in the comparison between **9** and **Zn9** as the *dom* mode has decreased. In the D_{ip}, a moderate decrease is seen in its value as a result of the Zn(II) metal insertion. This is highlighted in the decrease seen in the *bre* distortion mode.

Overall, at low substitutions (DEtTPP) there is an increase in *oop* distortion when a Zn(II) metal center is incorporated into the core. However, the opposite occurs in the *ip* distortion at this low substitution. As more ethyl groups are substituted onto the β-carbons of the Zn(II) porphyrins, there are decreases observed in both *oop* and *ip* distortions. The presence of an axial ligand only increases the *dom* distortion mode in the tTEtTPP (**Zn9**) and has no effect on the higher substitutions indicating no clear trend associated with axial ligands in these porphyrins.

Zn(II) chlorins: Similarly to the porphyrins, the Zn(II) metal in the core of the chlorins[28] increases the *oop* and decreases the *ip* conformations (Fig. S8). Chlorin **13** possesses the largest D_{oop} due to its large *sad* and *ruf* contributions as well as its significant *wav*(y) character whereas **14** has a slightly smaller D_{oop} which arises from its *sad* and *ruf* distortions. The DEtTPC, **13**, has the second smallest D_{oop} yet it has a large *sad* and a meaningful *ruf* and *wav*(y) conformations. The Zn(II) chlorin, **Zn13a**, has the smallest D_{oop} which is almost 1.000 Å smaller than **14**. This large decrease is due to the axial ligand preventing a large *sad* and shifting some *oop* distortion to the *dom* mode.

The *oop* distortion is almost inversely proportional to the *ip* distortion. To start off, **Zn13** has a much lower D_{ip} than **Zn13a**, **13** and **15**. The structure of **Zn13**'s *trn*(x), *trn*(y) and *bre* distortions contribute to the structure's D_{ip}, however, **Zn13a** has the highest D_{ip} distortion due to its large *bre* and considerable *N-str* conformation whereas **14** has the second largest D_{ip} due to it's the large *N-str* and *bre* character. The axial ligand, in this case, appears to greatly increase the *ip* distortion as well as decrease the D_{oop}. It is interesting to see the axial ligand cause an inverse relationship between the *oop* and *ip* conformations. The degree to which the axial ligand influences the 3D structure is already much clearer than seen in the porphyrin structures.

Upon increasing the number of ethyl groups on the periphery of these pentacoordinate chlorin macrocycles (**Zn17**), the *oop* distortion increases. This is solely due to the *sad* distortion increasing. The peripheral substitution pattern in **Zn17** is different from the free base chlorin (**16**). However, the *oop* distortion is still greater as shown by the NSD. The *ip* distortion however slightly decreases and this is most likely due to the *ip* distortion shifting from the *bre* mode to the *N-str* mode. It is clear once more that upon the increasing number of ethyl groups on the periphery of the heterocycle, an increase is seen in the D_{oop} while a decrease is seen in the D_{ip}.

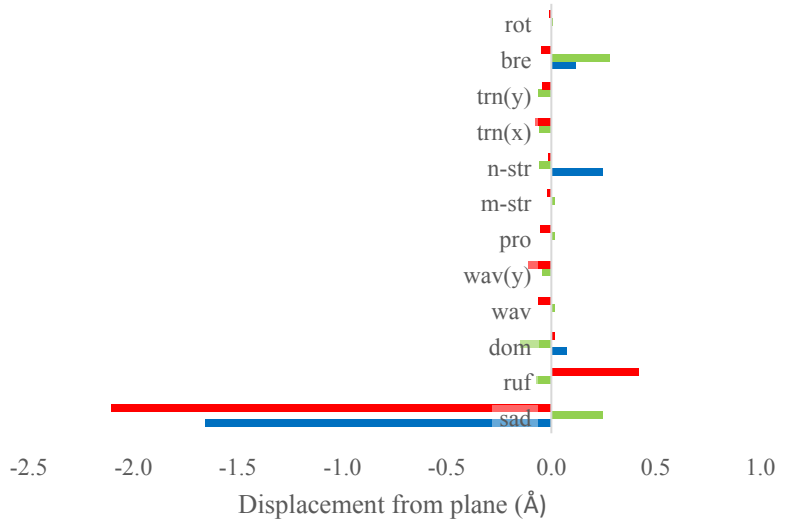

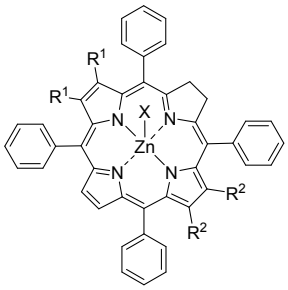

	CCDC	Color	R^1	R^2	X	Solvent	Ref.
Zn13	GELJAI		Et	H	-	No solvent	28
Zn13a	GELQET		Et	H	MeOH	DCM	28
Zn17	GELPIW		Et	Et	MeOH	DCM	28

Figure S8 Zn(II)XEtTPC series and NSD analysis of the X-ray crystallographic structures observed in the Zn(II)XEtTPC compounds listed in the table. Table contains their CCDC reference codes, the color corresponding to NSD graph, specific functional groups (R^1-R^2), axial ligands (X), and solvent in the respective unit cell.

2. Description of chlorophyll-related compounds NSD analyses

2.1 Phytochlorins

2.1.1 Free base phytochlorins

	CCDC	Color	R^1	R^2	R^3	R^4	R^5	R^6	Ref.
17a	MPOPHA		Me	Et	Me	CO_2Me	Me	$CH{=}CH_2$	33a
17b	MPOPHA02		Me	Et	Me	CO_2Me	Me	$CH{=}CH_2$	33b
17c	MPOPHA03		Me	Et	Me	CO_2Me	Me	$CH{=}CH_2$	33c
18	ROFVUE		CHO	Et	Me	CO_2Me	Et	$CH{=}CH_2$	33d
19^{i}	BIPBOR(N1-N4 ring)		Me	Et	Et	2H	Me	CH(OH)Me	33e
19^{ii}	BIPBOR(N5-N8 ring)		Me	Et	Et	2H	Me	CH(OH)Me	"
20	SOSZOP		Me	Et	COMe	2H	Me	CH(OH)Me	33f
21^{i}	BIPBIL(N1-N4 ring)		Me	^{i}Bu	Et	2H	Me	CH(OH)Me	33e
21^{ii}	BIPBIL(N5-N8 ring)		Me	^{i}Bu	Et	2H	Me	CH(OH)Me	"
22	BIXREF01		Me	$CH_2{}^{t}Bu$	Et	2H	Me	CH(OH)Me	33g

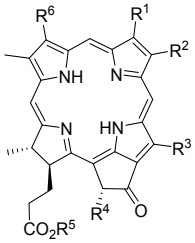

Figure S9 Free base phytochlorins and a table indicating their CCDC reference codes, the colour corresponding to the NSD graph, and specific functional groups (R^1-R^6). *Superscript i: N1-N4 ring in the crystal structure of the unit cell. **Superscript ii: N5-N8 ring in the crystal structure of the unit cell.

To begin, the free base phytochlorins (Fig. S9),[33] the D_{oop} as well as all of the *oop* distortion modes bar *pro* of **17a-c**, are very similar due to their identical structures. The D_{ip} of **17a-c** are approximately twice the displacement of the D_{oop} values of these compounds. This is indictive of highly planar free base compounds. As a result, there are several intermolecular reactions that occur as a result. The first and foremost is the π-stacking that is archetypical of this class of compound. This is primarily facilitated through the ester moieties interacting by short contacts, holding the packing structure in a head-to-head overlap configuration. The raise in D_{ip} in **18** compared to **17a-c**, is attributed to the larger *m-str* and *bre* distortions. These different configurations arise from hydrogen bonds and intermolecular interactions involving the CHO group, the meso-carbon, and the two ester groups as shown by the crystal structure's packing system. The introduction of the CHO group to R^1 aids the π···π interactions of the macrocycle through a short contact between the R^2 ethyl moiety, allowing for a tighter offset stacking pattern to occur between molecules. In the structure of **19^{i}** and **19^{ii}**, the methyl group is replaced by an ethyl group at the R^3 position, a hydrogen is changed for an ester at R^4, and an alcohol replaces the vinyl moiety at R^6. The combination of these changes results in a head-to-tail π-stacking pattern aided by short contacts between the oxo group at $C13^1$ position and the carbonyl group at R^6. The peripheral differences that occur in **19^{i}** and **19^{ii}** slightly increase all of the *oop* conformations, which is likely due to the ester group inducing a *ruf* conformation on the reduced pyrrole. The lower D_{ip} of **19^{i}** and **19^{ii}** is mainly represented by the lesser *m-str* and large *N*-str contributions. The large *N-str* conformations are likely due to the hydrogen bonding within the macrocycle core. The structure of **20** replaces the ethyl group at R^3 with an ester moiety, however, this does not impact the overall packing as the head-to-tail π-stacking between the oxo group at $C13^1$ position and the carbonyl group at R^6 is still present in the structure. The ester shows a small effect on the D_{ip} distortion modes with a general decrease in most D_{ip} modes in comparison to **19^{i}** and **19^{ii}**. This is combined with the *ruf oop* distortion mode. Similar to **19^{i}** and **19^{ii}**, **21^{i}** and **21^{ii}** correspond to two different molecules in the same structure. There are large *ruf* conformations, and like compounds **18** and **19$^{i/ii}$**, are a result of the head-to-tail π-stacking network between the oxo group at the $C13^1$ position and the carbonyl group at R^6. The *m-str, N-str,* and *bre* (*ip*) contributions are a result of the general peripheral substituents for this family of compounds. In the structure of **22**, the preference for *oop* modes moves towards the *dom* contribution. This structure is the only one to show such a large preference for this mode. By comparing the stacking pattern, it is clear that there is the overlapped stacking seen in **17-21**, which is a function of a co-facial intermolecular interaction that has now been swapped for an edge-on interaction between the molecules through the oxo group at the $C13^1$ position and the carbonyl group at R^6. While the head-to-head stacking still occurs in these domed macrocycles, it is a function of close packing and the bulkier group at the R^3 position. As seen previously in this series, the D_{ip} is larger than the D_{oop}. The *m-str*, *N-str* and *bre* conformations give rise to the large D_{ip}. In this group of compounds, it is apparent the *ip* contribution are much larger than the *oop* which suggest that the periphery substituents and the intermolecular interaction play more of a role in distorting the macrocycle than steric effects, which is typical for such compounds with a low number of peripheral substituents.

For the structure of **23**, there are two independent molecules in the crystal structure, **23^{i}** and **23^{ii}**.[34a] Between these chemically identical molecules, it is noted that **23^{ii}** has a larger D_{oop} than **23^{i}** which is expressed in the *sad* and *ruf* distortion modes. This significant difference between the molecules arises from the formation of atropisomers within the structure (**23^{i}** up-down-up-down; **23^{ii}** up-up-down-down; when considering the substituents on C2, C8, C17, C18). This results in a larger difference seen in **23^{ii}** by unbalancing the macrocycle ring. The inverse is seen in the *ip* distortion modes with the structure of **23^{i}** having larger contributions in all fields bar the *N-str* and *bre* modes. In the structure of **24**, the R^2 position has been replaced by an oxo group and the R^3 position by an ester.[34b] In this structure, there are three sets of intermolecular interactions that form the full packing pattern. The first is an edge-on interaction between the oxo group at the $C13^1$ position and the hydrogens of the ethyl, methyl and meso carbons between the N2 and N3 pyrrole units. This creates a planar sheet of macrocycle rings in a zig-zag pattern. This is coupled with a second type of intermolecular interaction in the form of offset π-stacking between the macrocycle rings in a head-to-head fashion. The final feature of the crystal packing is a group of head-to-head short contacts between the ester moieties that hold individual planes at a ~45° angle to each other in the structure. In comparison to compound **23^{ii}**, there is a moderate decrease in both the *dom* and *ruf* distortion modes with a large decrease in the *sad* mode. However, compared to **23^{i}** there is a slight increase seen in these modes, but they exhibit similar D_{oop} contributions. The *ip* distortion modes are only slightly lower than that of **23^{i}** or **23^{ii}**. In the structure of **25**, the ethyl group at the R^1 position is replaced by a fluorinated ester.[34c] This results in three packing groups that make up the overall packing. The first is the head-to-head overlapped π-stacking between the macrocycle rings which is aided by H···F short contacts between the R^1 groups and an O···H interaction between the R^3 moieties. The second packing group is between the fluorine atoms and the R^1 ester's methyl hydrogen of R^3 moiety which holds the macrocycles in a face-to edge pattern. The final packing pattern seen is between the oxo group at the $C13^1$ position and the ester hydrogen atoms of the R^3 group that form a rotated head-to-head interaction. In this structure, the overall D_{oop} is slightly lower than that of **23$^{i/ii}$** and **24**, showing a decrease in all *oop* modes compared to one or the other of these

structures. In the *ip* distortion modes, compound **25** shows a slight increase in the D_{ip} over **23**$^{i/ii}$ and **24** with its largest contribution seen in the *bre* mode. In summary, the addition of an oxo group to the C13^1 position shows a slight decrease in *oop* and *ip* distortion modes however the most of this effect is counteracted by the addition of the fluorinated ester to the R^1 position. Similar to compounds **17-22** above, π···π interactions are quite prevalent due to the ostensibly planar macrocycles. However, the inclusion of short contacts of specific functional groups, also play a role in favoring certain distortion modes in the NSD profiles.

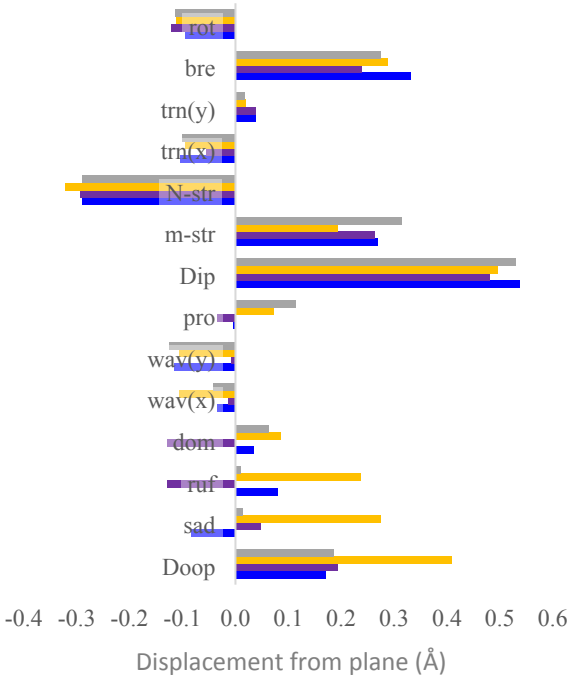

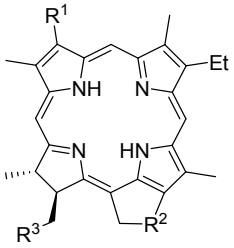

	CCDC	Color	R^1	R^2	R^3	Ref.
23i^i	RIWNIU (N1-N4 ring)		Et	CH_2	Et	34a
23i^{ii}	RIWNIU (N5-N8 ring)		Et	CH_2	Et	"
24	KOVXUO		Et	C=O	CH_2CO_2Me	34b
25	PEPJUR		$C_5H_5F_3O_2$	C=O	CH_2CO_2Me	34c

Figure S10 Free base phytochlorins series and NSD analysis of the X-ray crystallographic structures observed in the free base phytochlorins compounds listed in the table. Table contains their CCDC reference codes, color in NSD graph, and specific functional groups (R^1-R^3) in their unit cell.

2.1.2 Metallated phytochlorins

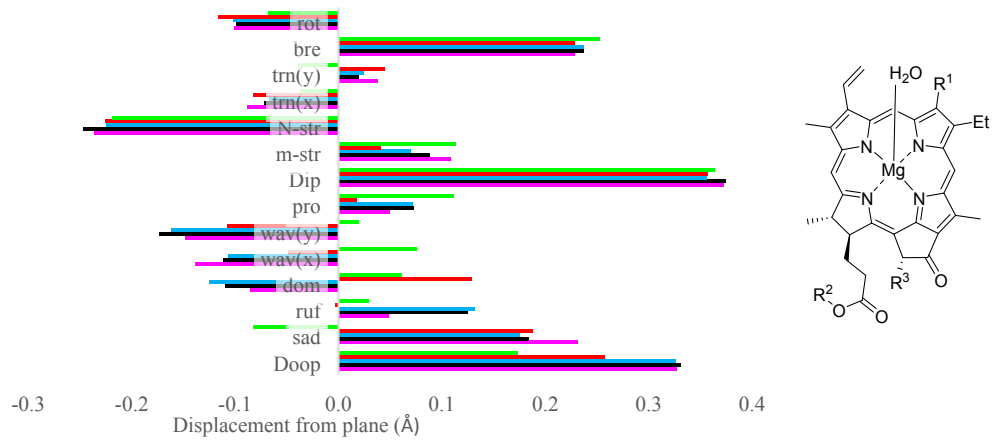

	CCDC	Color	R^1	R^2	R^3	Solvent	Ref.
26	MPCHLM10		Me	Me	2H	Et_2O	35a
27	MCLPHD10		Me	Me	CO_2Me	H_2O	35b
28a	AECLPA01		Me	Et	CO_2Me	H_2O	35c
28b	AECLPA10		Me	Et	CO_2Me	H_2O	35e
29	ECPHBH		CHO	Et	CO_2Me	H_2O	35d

Figure S11 Mg(II) phytochlorins series and NSD analysis of the X-ray crystallographic structures observed in these Mg(II)phytochlorins compounds listed in the table. Table contains their CCDC reference codes, color in NSD graph, specific functional groups (R^1-R^3), and the solvents within the respective unit cells.

These low distortions in the Mg(II) phytochlorins (Fig. S11) (**26-29**)[35] are most likely due to the one intermolecular hydrogen bond between the axial water ligand and carbonyl functionality in the plane of the macrocycle. With regards to published protein structures containing chlorophyll compounds, there are several features that are key which are represented in the solid-state structures above. While all the above compounds exhibit a substantial amount of close contacts and hydrogen-bonding based of the substitution type and conformation, it is the metallophytochlorins which closely represent conformations expected in the peridinin–chlorophyll-protein structures. This is seen through the Mg axial ligand (H_2O in this case) coordinating either directly or through the solvent present to form a hydrogen-bonded network to the ester or oxo group at the $C13^1$ position of the macrocycle skeleton. This is reminiscent of His-66···(H_2O)···Mg coordination that is seen in Chl a as reported by Schulte *et al.*[40] In this series of compounds, there is very little change to the D_{ip} distortion mode with only compound **26** showing significant reductions in the *rot* and *trn*(x) modes potentially due to not having an ester present on the R^3 position, similar to **27-29**. This is also represented in the *oop* distortion modes with compound **26** having significantly less contribution to all modes bar the *pro* due to the induction effect the ester group has on the macrocycle skeleton. Also, in the structure of **26**, the ester at position C17 on the reduced pyrrole ring is shown to point above the macrocycle plane. In this series, this is the only time this occurs and there are no short contacts including this ester group. The only short contacts are seen between the axial water ligand and the Et_2O solvent on one side of the macrocycle combined with an O···H interaction between the axial water ligand and the oxo group at the $C13^1$ position of the macrocycle, forming a step-like π-stacking pattern. Moving to the structure of **27**, an acetyl group now occupies the R^3 position and the solvent included in the structure has changed from Et_2O to water. While the addition of an acetyl group has minimal changes on the *ip* distortion modes as mentioned before, there is no evidence of this group forming short contacts or changing the overall structure in any significant manner. The most obvious changes occur with the solvent water molecules. In this case, the solvent water molecules acts like a bridge between the axial ligand and the ester at the C17 position of the macrocycle creating a tighter offset layered packing pattern. The *dom* character appears to be more prominent in this structure than **26** even though they both possess very similar axial hydrogen bonds. This can be credited to the water solvent that is now present in this crystal structure. The *dom* character increases by a factor of approximately twenty as the solvent in the crystal structure changes. The water solvent interacts with the water axial ligand *via* hydrogen bonding and appears to 'pull' the Mg(II) metal out of the plane and thus creating a *dom*-like configuration. The structures of **28a** and **28b** while being chemically identical, have two subtly different packing patterns. Both compounds **28a** and **28b** have a similar packing style to **27** however, the acetyl group is now occupying one side of the axial water ligand of the same macrocycle ring rather than the R^3 ester of the nearest neighbor. A new short contact is present between the oxo group at $C13^1$ position and the CH_2 of the R^3 ester. However, with this change, there is little difference in the overall packing of the structure. In the NSD, **28b** has the larger D_{oop} than **28a** due to the meaningful contributions in all of the *oop* modes except the *dom* and *ruf* modes. It also has the largest D_{ip} in this series as a result of the considerable *N-str* conformation. The structure of **29** contains a CHO group at the R^1 position, however, as this group is co-planar to the macrocycle ring, it is occupied by an intramolecular hydrogen-bond with the meso-hydrogen atom and does not significantly contribute to the overall packing. This does affect the *m-str* and *trn*(x) by showing a slight increase compared to compounds **28a** and **28b**. The structure of **29** has the largest contribution to the *sad* distortion mode and this can be attributed to a small change observed in the packing of this compound. The solvent water molecule is seen to form the same bridge between the acetyl group and the axial water ligand, but now also has a third contact between the ester at position C17 of the phytochlorins above in an elaborate hydrogen-bonding fashion. Overall, while the *ip* distortion mode are all similar in this class of compounds, there is a clear increase seen in the *oop* modes as a result of peripheral substitution type and size coupled with changes seen in the type of interaction involving the included solvent.

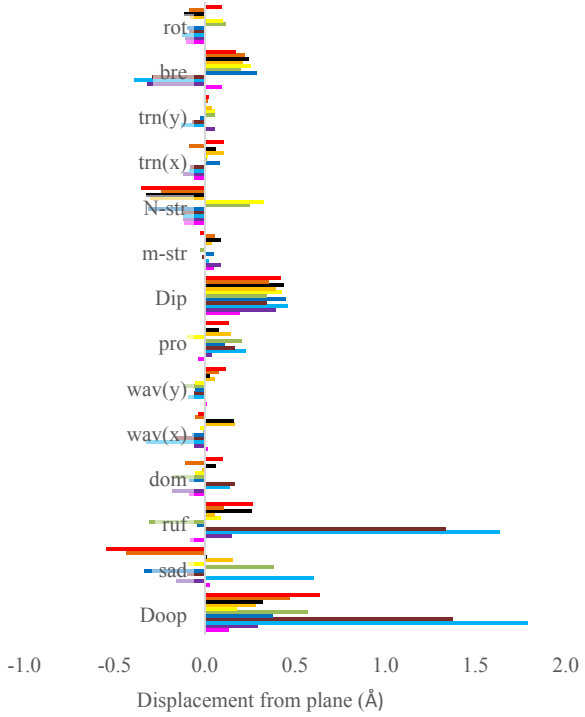

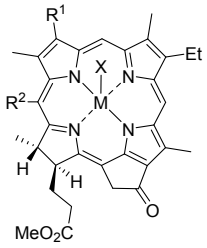

	CCDC	Color	M	R^1	R^2	X	Solvent	Ref.
30	CELRIU		Zn(II)	CH=NOH	H	O=C13[1]	$CHCl_3$	36a
31	MEHGUD		Zn(II)	$COCH_3$	H	O=C17[3]	CH_2Cl_2	36b
32^{i*}	XOKGOV(N1-N4 ring)		Zn(II)	$C_{13}H_8N$	H	3-pyr	Et_2O, THF	36c
32^{ii**}	XOKGOV(N5-N8 ring)		Zn(II)	$C_{13}H_8N$	H	3-pyr	Et_2O, THF	"
33^{i*}	MIBJEO(N1-N4 ring)		Zn(II)	C_7H_6N	H	3-pyr	CH_3CN	36d
33^{ii**}	MIBJEO(N5-N8 ring)		Zn(II)	C_7H_6N	H	3-pyr	CH_3CN	"
34	ZOKMAP		Zn(II)	oxazole	H	N-oxazole	Toluene	36e
35	HAHBAT		Ni(II)	$CH=CH_2$	H	-	-	16
36	YOVYAJ		Ni(II)	Et	Me	-	-	37
37	UMAZAJ		Cd(II)	CH_2OH	H	OH 3[1]	-	38a
38	KILQAZ		Pt(II)	Et	H	-	-	38b

Figure S12 Metallated phytochlorins, NSD analysis of the X-ray crystallographic structures observed in these metallophytochlorins compounds listed in the table. Table contains CCDC reference codes, color in the NSD graph, metal (M), specific functional groups (R^1-R^2), axial ligands (X), and solvent present in the respective unit cell. *Superscript i: N1-N4 ring in the crystal structure of the unit cell. **Superscript ii: N5-N8 ring in the crystal structure of the unit cell.

The Mg(II) phytochlorins are more naturally occurring than other types of metals in the core of these chlorophyll compounds.[1] The most common metal observed in the core of metallated pheophorbide derivatives according to the CSD is Zinc(II).[29–33] The NSD profile of the Zn(II) structures in this section as well as the two Ni(II), one Cd(II), and one Pt(II) structures will be discussed herein. These metal complexes are shown in Fig. S12. The axial ligand bound to the Zn(II) metal in **30** is the oxo group of another molecule of **30**. The oxygen acts as an 'intramolecular axial ligand" in the 3D structure and also plays a large role in the large *N-str* input observed. Coupled with this is the top-and-tail hydrogen-bond network that is formed between the R^1 substituent and the ester. By substituting the R^1 group for a carbonyl (**31**), this top-and-tail network is removed and the ester at C17 position now acts as the axial ligand rather than the C13[1] oxo group.

The second independent molecule in XOKGOV (**32**^{ii}) has a slightly lower D_{oop} than the first independent molecule (**32**^{i}) because of the 0.204 Å decrease in the normal *ruf* deformation, even though the *sad* mode has increased. The D_{ip} has also slightly increased but is caused by slight deviations in *N-str* and *bre* contributions. In the structure of **32**$^{i/ii}$, the formation of atropisomers gives rise to the two independent molecules. In the case of **32**^{i}, the ester is pointing in the same direction as the axial ligand (above the plane) while in **32**^{ii} the ester is pointing in the opposite direction (below the plane). This results in the small difference seen in D_{oop} and D_{ip} distortion modes of these compounds. In the structure of **33**$^{i/ii}$ while the D_{ip} are quite similar there is a notable difference in the D_{oop} with a three-fold increase in contribution from **33**^{i} to **33**^{ii}. While being chemically identical, there are two things to note. The first is that **33**^{i} axial ligand is the pyridyl unit of **33**^{i} and the same for **33**^{ii}. The second is that the solvent acetonitrile only interacts with the core and peripheral substituents of **33**^{i}. This suggest that the decrease in D_{oop} is a result of solvent interactions in the structure packing. These raised distortion modes in **34** are due to the oxazole peripheral substituent now acting as an axial ligand creating a face-to-edge packing pattern.

The *peri*-interactions introduced by the methyl group at the meso-position of the phytochlorin **36**, increases the *sad* contribution by 0.504 Å. The π-interactions in the packing system of **36** (YOVYAJ) increase the *ruf* by 0.297 Å. This is mainly due to the tension in the distorted macrocycle of **35** as shown by the larger *bre* contribution. The other main factor is Ni(II) contracting the core of **36** to a greater extent than

35 (3.831 Å vs 3.8655 Å, respectively). Other factors are the removal of the methyl group at the R^3 meso position and the substitution of an ethyl group for an alcohol at R^1. The alcohol coordinates to the Zn(II) metal in a similar fashion as seen in the Zn(II) phytochlorins. The *oop* modes, except *wav*(y) and *pro*, are all smaller in **38**[38b]. The *N-str* and *bre* contributions are far smaller in **38**. The more planar structure of the Cd(II) phytochlorin, **37**,[38a] exists due to the planar head-to-tail style packing.

Overall, the main differences observed is that the Ni(II) phytochlorins have by far the largest *oop* distortion due to the large Ni(II) induced *ruf* distortion mode. The large D_{oop} also obtains significant contributions from the *sad*, *wav*(x) and *pro* modes. The D_{ip} character in the Ni(II) derivatives arises from the *bre* mode. The Zn(II) phytochlorins have a lower D_{oop} displacement but a larger *ip* distortion thanks to the bigger *N-str*. As seen in the test case, this is due to the Zn(II) metal contracting the Zn(II)-Nitrogen bond. The heavy atom phytochlorins, **37** (Cd(II)) and **38** (Pt(II)) have small *oop* and *ip* distortions. Which suggests that the heavier the atom, the smaller the distortion due to a π-aggregation and head-to-tail style "flat" packing.

2.1.3 Free base phytochlorin exceptions

Two phytochlorins, where ring E has been altered, are shown in Fig. S13. The D_{oop} of **S1** (FOXTUH) is 0.084 Å lower than **S2** (FOXWIY).[39] The differing D_{oop} values can be attributed to O_1 on the fused ring in **S1**. The structures are less distorted in the *oop* modes and the *ip* modes have a more significant impact on the 3D structure as shown by the high *bre* values (Fig. S13). This difference is spotted by the NSD as there are higher *sad* and *ruf* distortions in **S2** than **S1**.[39] With the inclusion of these rings, there is 'rigidity' observed in the NSD. By analyzing the crystal packing system of **S1**, the oxygen on the oxo group is participating in intermolecular hydrogen-bonding with the ester of another molecule according to the crystal structure, therefore forcing the ester to be more non-planar than the ester group in **S2**.

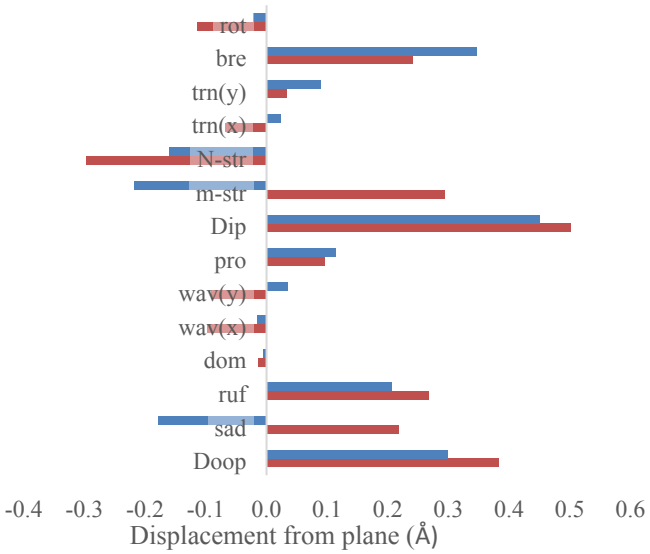

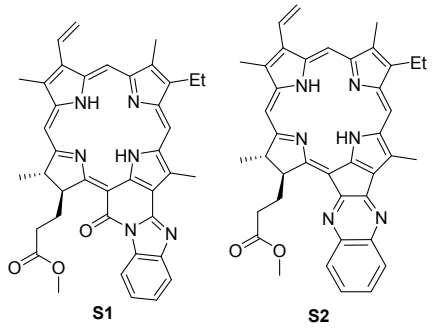

	Color	CCDC	Ref.
S1		FOXTUH	39
S2		FOXWIY	39

Figure S13 Two free base phytochlorins with ring systems conjugated to the macrocycle, NSD analysis of the X-ray crystallographic structures of the free base phytochlorin compounds, and a table indicating their color in the NSD graph, and CCDC reference codes.

2.2 Bacteriochlorophyll-related structures

The *ip* distortion modes of the bacteriochlorophyll compounds (**39a-c**, WIKSEO, BAVSUM01, and BAVSUM)[40] have larger displacements than the main *oop* distortion mode, the *sad* distortion. The oxygen containing β-substituents in the dihydrophytochlorin section generally demonstrate large *ruf* distortions due to the hydrogen bonding networks, therefore, causing non-planarity. This *ruf* character is absent in the bacteriopheophorbide a structures. Bacteriopheophorbide a compounds are bacteriochlorins and their NSD profile suggests that the D_{oop} range is much smaller than in the free base phytochlorins. The larger D_{ip} values arise from the large *m-str*, *N-str,* and *bre ip* modes. The most common feature in the packing of these structures is the π-stacking between the macrocycle rings.

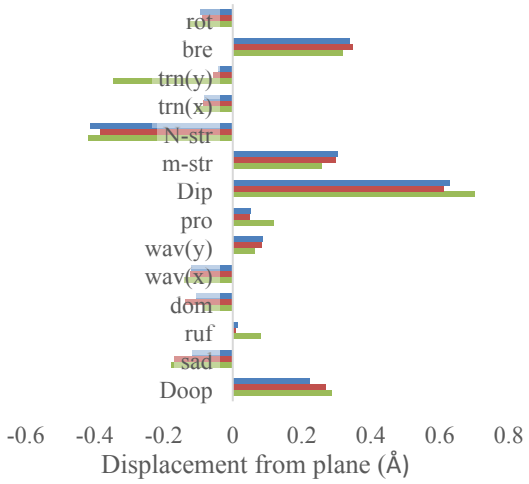

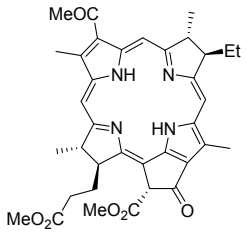

	Color	CCDC	Solvent	Ref.
39a		WIKSEO	-	40a
39b		BAVSUM01	C_6H_6	40b
39c		BAVSUM	C_6H_6	40c

Figure S14 Bacteriopheophorbide a structures and the NSD analysis of the X-ray crystallographic structures observed in these bacteriopheophorbides. Table contains the color in the NSD graph, CCDC reference codes, and the solvent within the respective unit cell.

2.3 Chlorins

2.3.1 Free base chlorins

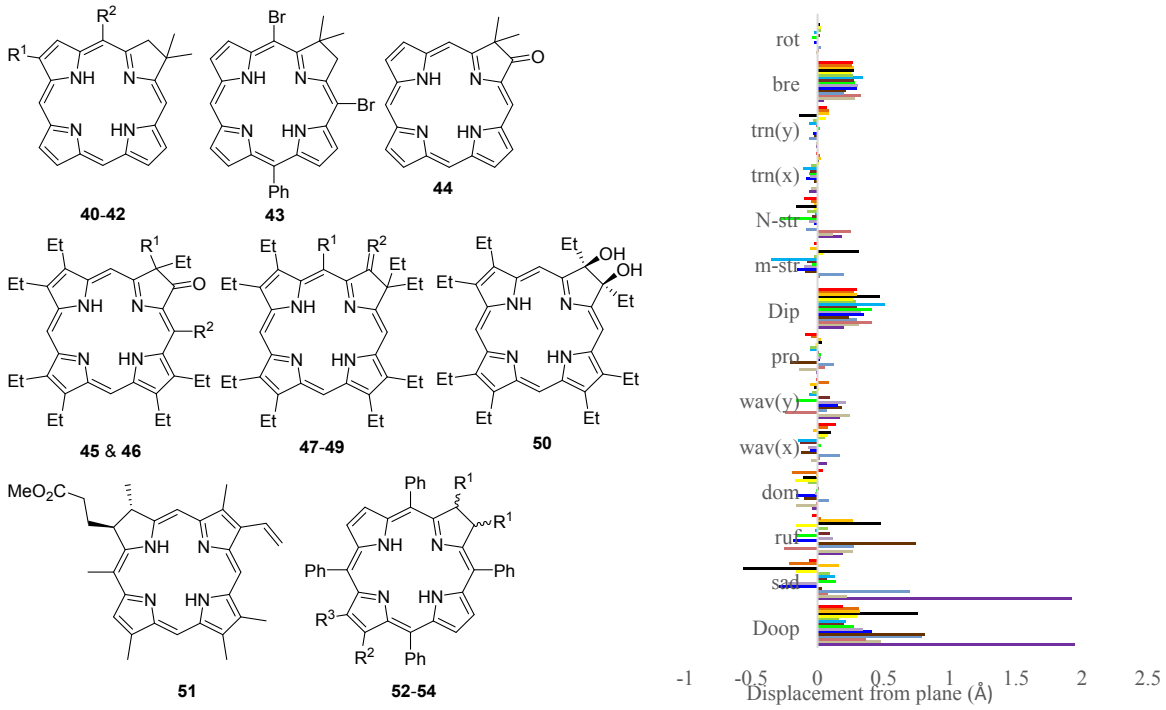

	CCDC	Color	Solvent	R^1	R^2	R^3	Ref.
40	PACRES		-	H	H	–	42a
41	PACRIW		-	Br	H	–	42b
42	MUMGAD		-	COMe	Br	–	42b
43	TACTID		-	–	–	–	42c
44	PACROC		–	–	–	–	42a
45	WANDEX		-	OH	–	–	42d
46	WANDAT		–	Et	Cl	–	42d
47[i]	WANBOF		–	H	O	–	42e
47[ii]	WANBOF		–	H	O	–	42e
48	WANCAS		$CHCl_3$	H	N-OH	–	42e
49	WANCEW		$CHCl_3$	OCHO	O	–	42f
50	KOCZUX		$MeCO_2Et$	–	–	–	42g
51	PHLLCL10		–	–	–	–	42h
52	NOCGER		$CHCl_3$, MeOH	$CH(CN)_2$	Br	Br	42i
53	QAKLUJ		DCM	*n*Bu	H	H	42j
54	TIPBIF		EtOH, H_2O	OH	NO_2	H	42k

Figure S15 Free base β-substituted chlorins and NSD analysis of the X-ray crystallographic structures observed in these free base chlorins listed in the table. Table contains their CCDC reference codes, the color corresponding to the NSD graph, solvent within the respective unit cell, and specific functional groups (R^1-R^3).

2.3.2 M(II) β-substituted chlorins

To begin the discussion of the metallated β-substituted chlorins, the structures as well as the NSD data are shown in Fig. S16. The insertion of the Zn(II) metal into **40** yields **S3**, NIDFEM)[43a] and the D_{oop} is slightly increased due to the rise in *sad* contribution compared to the free base chlorin, but the largest difference is seen in the *dom* and *wav*(y) conformations. The D_{ip}, however, has slightly decreased upon metal insertion due to the contraction of the Zn(II)-Nitrogen bond as shown in the test case. This is due to the decrease in the *bre* contribution to the *ip* distortion of the Zn(II) chlorin. Comparing the differing Zn(II) structures of **S3** and **S4** (XIPLEO),[43b] there is a large surge in the D_{oop} that stems from the raised *oop* distortion in all modes bar the *wav*(y). This is brought about by the introduction of a meso-tolyl group and a bromine atom that is trans to the periphery of the chlorin. These introductions, however, decrease the D_{ip} as they inhibit the *N-str* and *bre* distortions. As shown in the free base chlorin section and the phytochlorin section, the presence of the oxygen on the periphery as well as this oxygen being the axial ligand, increases the D_{oop} as shown in the increase from **S3** to **S5**. In this case however, it is not as high as the distortion of macrocycles with *peri*-interactions (**S4**). Comparing **S5** (NIDFAI)[43a] to its free base counterpart **44** (PACROC), the presence of the Zn(II) metal in the core raises the D_{oop} and lowers the D_{ip}. There are higher *sad* and *ruf* conformations but a smaller *dom* configuration in **S5**. There is a smaller *bre* normal deformation which is the cause for the lower D_{ip}. The presence of a Fe(II) metal with a nitro group as the axial ligand (**S6-1**; QUJZUQ)[43c] instead of a Zn(II) in the core, slightly decreases the D_{oop} but drastically reduces the *ip* distortion as the D_{ip} is 0.152 Å less in **S6-1** compared to **S5**. Changing the axial ligand from nitro (**S6-1**) to a chlorine (**S6-2**, LAMDUZ)[43e] increases the D_{oop} by

0.213 Å. This is reflected by an increase in the *sad* and *wav*(x) *oop* distortion modes for **S6-2** as a result of moving to an electron withdrawing axial ligand.

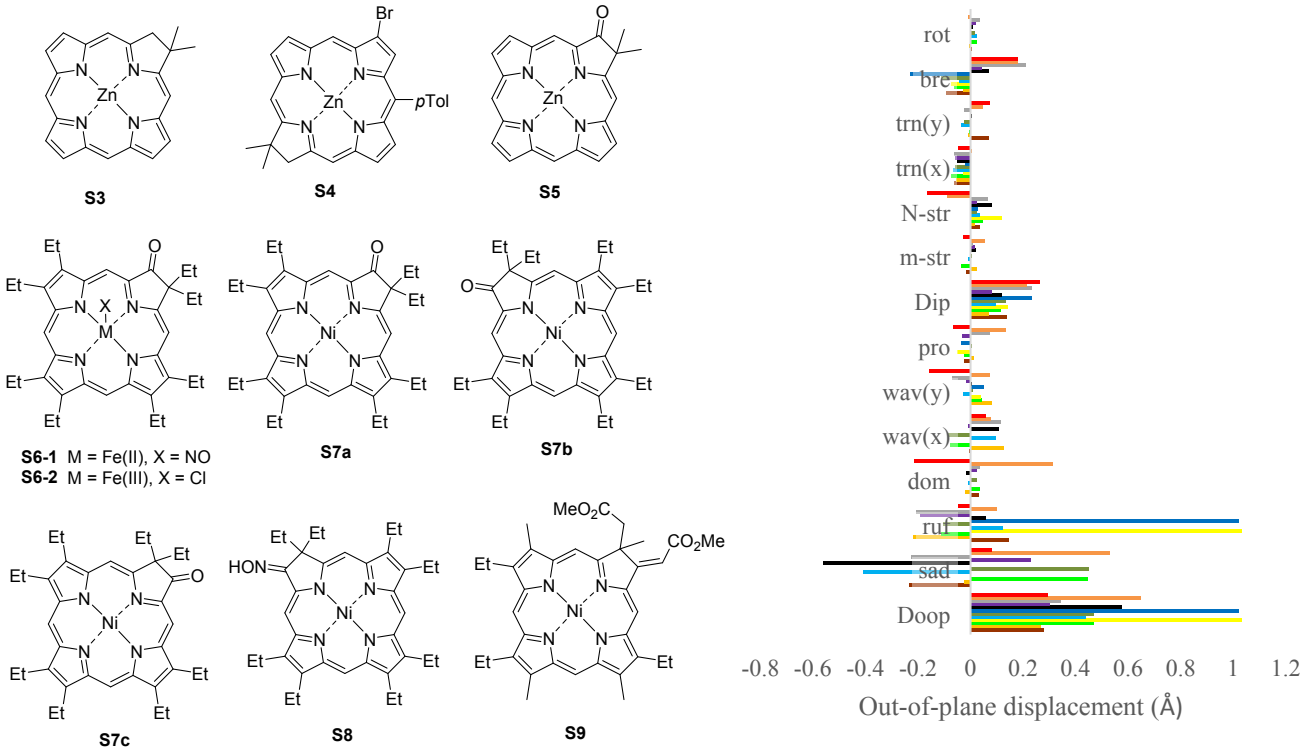

	CCDC	Color	Metal	Axial Ligand (X)	Solvent	Ref.
S3	NIDFEM		Zn(II)	–	C_6H_{12}	43a
S4	XIPLEO		Zn(II)	–	$CHCl_3$	43b
S5	NIDFAI		Zn(II)	···O=C	C_6H_{12}	43a
S6-1	QUJZUQ		Fe(II)	NO	$CHCl_3$	43c
S6-2	LAMDUZ		Fe(III)	Cl	$CHCl_3$	43e
S7a^{i}	DOZVIX01 (N1-N4)		Ni(II)	–	–	43d
S7a^{ii}	DOZVIX01 (N5-N8)		Ni(II)	–	–	43d
S7b	DOZVIX02		Ni(II)	–	–	42e
S7c^{i}	DOZVIX (N1-N4)		Ni(II)	–	–	43f
S7c^{ii}	DOZVIX (N5-N8)		Ni(II)	–	–	43f
S8	WANBIZ		Ni(II)	–	C_6H_{14}, C_5H_{12}	42e
S9	JUNZUN		Ni(II)	–	MeOH	43g

Figure S16 Metallated β-substituted chlorins series and the NSD analysis of the X-ray crystallographic structures observed in the metallated β-substituted chlorin compounds listed in the table. Table contains their CCDC reference codes, the color corresponding to the NSD graph, metal in the chlorin core, axial ligand attached to this metal, and the solvent within the respective unit cell.

The introduction of a Ni(II) metal into the core instead of a Fe(II) causes a rise in non-planarity compared to the Fe(II) chlorins studied (**S6-1**). In the first independent molecule of the structure with CCDC reference code DOZVIX01 (**S7a^{i}**), a Ni(II) metal in the core increases the D_{oop} by 0.719 Å.[43d] This is not the case however for the second independent molecule (**S7a^{ii}**). There is a large difference between the 3D structure of **S7a^{i}** and **S7a^{ii}**. This is realized by the formation of atropisomers in the crystal structures. In the case of **S7a^{ii}**, all β-substituents point in the same direction. However, for **S7a^{i}**, the β-substituents are alternating in the direction they point (above or below the macrocycle plane) which gives rise to a larger *ruf* distortion (nearly 1 Å). This structure also has the largest D_{ip} in the series of structures with DOZVIX CCDC reference codes, because of its large *bre* character. The crystallization of a Ni(II) chlorin that has the carbonyl and two ethyl groups on a different pyrrole to both molecules of **S7a**, yields the structure of DOZVIX02 (**S7b**).[42e] This structure has a large *sad* distortion as well as meaningful *ruf* and *wav*(x) contributions. This chlorin has the smallest D_{ip} due to the presence of the smallest *bre* distortion mode. Upon analyzing **S7a**, exchanging the carbonyl and the ethyl positions on the same pyrrole yields the 3D crystal structures of the two molecules in DOZVIX01 (**S7c^{i}** and **S7c^{ii}**).[43f] The first molecule, **S7c^{i}**, has the largest D_{oop} in this "DOZVIX" series. It is marginally larger than that of **S7a^{i}** almost solely due to its slightly larger *ruf* configuration. It has a much smaller D_{ip} due to its largest *N-str* distortion mode. The second molecule, **S7c^{ii}**, has a far smaller D_{oop} as it has small contributions from all modes, the largest stemming from the *sad* and *wav*(x). This structure has the second smallest D_{ip} even though it has the largest *m-str* and *trn*(x). The small *bre* in this structure is largely responsible for the small D_{ip}. Similarly, to **S7a$^{i/ii}$**, all of the β-substituents in **S7c^{ii}** point in the same direction and in **S7c^{i}**, the β-substituents are alternating in

the direction they point (above or below the macrocycle plane). This atropisomer formation gives rise to the difference seen between the two molecules in their NSD profiles.

In WANBIZ (**S8**),[42e] the chemical differences between this structure and **S7a** are the presence of the hydroxylamine at the periphery instead of the oxygen as well as the switching of the ethyl groups and the sp^2 carbon location (**Fig. S16**). The D_{oop} decreased by an average of 0.747 Å upon this transformation as the *sad* and *ruf* contributions decreased. Similar to **S6-1**, the D_{ip} has dramatically decreased because of the small *bre* configuration. In the crystal structure of **S8**, the macrocycles form head-to-head dimers through a hydrogen-bond with the NOH group. These dimers are slightly rotated to one another and do not allow for sufficient overlap to form π-stacking.

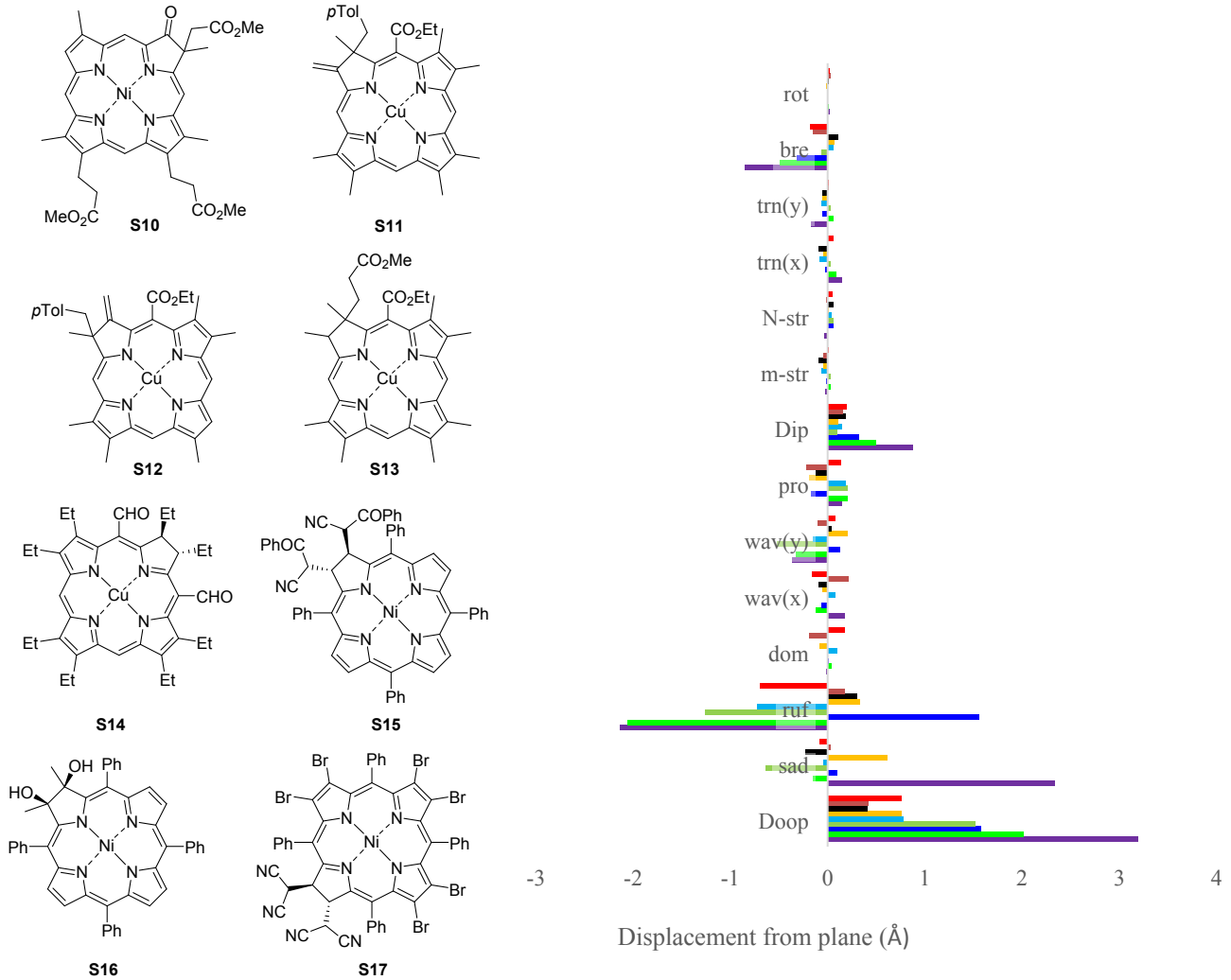

	CCDC	Color	Solvent	Ref.
S10[i]	PASXEM (N1-N4 ring)		–	44a
S10[ii]	PASXEM (N5-N8 ring)		–	44a
S11	NIJBOX		–	44b
S12	NIJBUD		–	44b
S13	LICSEV		–	44c
S14	LOGYAH		–	44d
S15	XANDOI		–	44e
S16	ZAZNOF		–	44f
S17	NOCGAN		$CHCl_3$	42i

Figure S17 Further metallated β-substituted chlorins series and the NSD analysis of the X-ray crystallographic structures observed in the metallated β-substituted chlorin compounds listed in the table. Table contains their CCDC reference codes, the color corresponding to the NSD graph, and the solvent within the respective unit cell.

The structure of **S9** (JUNZUN)[43g] has one of the lowest D_{oop} values in this series. It is similar to the D_{oop} of **S8**, even though the structures are not as similar. The *sad* and *ruf* conformations have decreased and the D_{ip} is similar to **S7c** with similar contributions. In this structure, the ester on the 8 position is held co-planar to the macrocycle ring and the ester on the C7 position is held perpendicular. This allows for a reciprocated short contact interaction between these two groups holding the macrocycle in an optimum position to π-stack. In this series, it appears that not only is the type and number of peripheral substituents crucial, but also the orientation in which they point (either above, below, or co-planar), is also important for overall contribution towards *ip* and *oop* distortions.

The second group of metallochlorins is shown in Fig. S17. The introduction of more polar peripheral substituents has increased the D_{oop} of the macrocycles of **S10** (PASXEM (N1-N4 ring) and PASXEM (N5-N8 ring)),[44a] compared to **S9** by 0.481 and 0.137 Å, respectively. The difference in the values of the D_{oop} is a result of both esters pointing in opposite directions in the N1-N4 ring whereas in the N5-N8 ring, both esters point in the same direction which is a feature that has been seen above. These rises in the D_{oop} represent the increase in the *ruf* and *dom* conformations. These polar groups also increase the D_{ip} as there is a higher *bre* configuration in **S10^{i}** and **S10^{ii}**, according to the NSD profiles.

The metallated chlorins **S11** and **S12**, while similar in chemical composition, differ in the orientation of the peripheral substituents. This results in two distinct packing patterns. The first, **S11**, favors a head-to-tail tightly packed structure, whereas **S12** forms a loose edge-on packing system. This causes the D_{oop} of **S12** (NIJBUD) to be 0.347 Å larger than that of **S11** (NIJBOX).[44b] The D_{ip} of **S12** is lower than the D_{ip} of **S11** because of the lower *bre* distortion mode in **S12**. The Copper(II) complex **S13** (LICSEV)[44c] has a slightly larger D_{oop} than **S12** as the ester group on the reduced pyrrole induces a larger *ruf* distortion that arises from intermolecular hydrogen bonding. The D_{ip} has also been slightly enhanced due to the higher *m-str* and *N-str* configurations.

The structures of LOGYAH (**S14**)[44d] and NOCGAN (**S17**)[42i] have large *sad* and *ruf* normal deformations. However, in the other two structures of XANDOI (**S15**) and ZAZNOF (**S16**),[44e, 44f] this dramatic increase in distortion arises solely from the large *ruf* conformation. To conclude, a Ni(II) metal generally induces a large *ruf* conformation that is responsible for the large D_{oop} shown above. The D_{ip} of **S14** contains little to no distortion compared to **S15-S17** that all have large D_{ip}s due to the extensive *bre* conformations present.

Overall, the presence of a metal and an axial ligand in the core of the β-substituted chlorin increases the non-planarity. Depending on the metal and peripheral substituents, different *oop* distortions can be realized. A similar scenario is seen in the *ip* distortion modes as the *bre* and *N-str* conformations best represent the D_{ip}. The second macrocycle in DOZVIX01 (**S7a^{ii}**) has different contributions to the D_{oop} and D_{ip}. This 24-atom mean-plane's main conformation of the *oop* modes is *sad* whereas the main normal deformation in the *ip* modes is the *bre* mode. In **S11**, the *p*-methylbenzyl group, adjacent to the ester group on the meso-position of the chlorin, can orient away from this ester and thus not create such a large *peri* interaction. In **S12**, the rigid sp^2 hybridized carbon adjacent to the ester group creates a larger *peri*-interaction thus creating a larger *sad* contribution. The D_{oop} of **S14** and **S15-S17** have dramatically increased due to the increased number of *peri*-interactions that arise from the increased number of peripheral substituents as discussed in the chlorin section of the test case. In the test case however, the increasing number of substituents increased the *sad* distortion in almost all cases.

2.3.3 Fused chlorins

First, we look at the compound shown in Fig. S18. In this series, the archetypical description for their structures is a high π-stacking with the fused moieties on opposite sides. There are subtle differences from structure to structure which will be discussed in turn and these differences along with the alternate peripheral substituents give rise to changes in their NSD profiles. When a fused benzene ring is introduced to the chlorin as in the structure of **S18** (JUNZIB),[43g] this yields a D_{oop} of 0.268 Å. In the structure of **S18**, a considerable head-to-tail π-stacked overlap with the fused rings as far apart as possible is shown. This *oop* distortion arises from the *sad* and *ruf* contributions. There is more *ip* character in the 3D structure of **S18** as the D_{ip} has significant *m-str*, *N-str* and *bre* conformations. The substitution of an ester onto the fused benzene in **S18** yields the structure of **S19** (QIRHEE).[45a] The inclusion of this ester group drastically changes the packing of the structure from the π-stacked pattern to a face-to-edge pattern. This results in a decrease in the D_{oop} and D_{ip} due to a lower *sad* conformation in the *oop* modes and a lower *m-str* conformation in the *ip* modes. Moving to the structure of **S20** (OEBPNI), which is similar to **S18** with a Ni(II) center included. Fused chlorin, **S20**, contains more *ruf* character than **S18** as a result of the inclusion of the metal center and this results in a tight head-to-head packing pattern.[45b] In the structure of **S21** (VUFTEV),[45c] the α,β-unsaturated aldehyde increases the D_{oop} of the structure even further than **S20** due to peripheral interactions. These interactions force the structure to adopt a head-to-tail overlap coupled with a face-to-edge packing in the structure. These interactions thus cause a large *bre* conformation as there is a significant expansion in the 24-atom mean-plane.

Using the structure of **S18** as the parent compound, the substitution of an amide onto this structure instead of one of the ethyl groups adjacent to the benzene, as well as placing an ethyl group on the benzene results in an insignificant decline in the D_{oop} of **S22** (XIXVAB).[45d] In the structure of **S22**, this is represented by a head-to-head overlap caused hydrogen-bonding between the amide groups. This is coupled with the face-to-edge interaction as a result of the non-classical hydrogen-bond between the fused benzene ring and the oxygen of the amide group. There is a meaningful decrease in *sad* distortion however and there is a rise in the *wav*(y) mode. The lesser D_{ip} represents a larger difference as the *bre* distortion decreases by 0.115 Å. The introduction of an amide slightly decreases the *oop* distortion and meaningfully decreases the *ip* distortion. Breaking the aromaticity of the fused ring to the chlorin is one reason for the large increase in the D_{oop} between **S22** and **S23** (XIXTUT).[45d] The packing patterns of these two structures is quite different with **S23** exhibiting a head-to-tail overlap combined with the face-to-edge interaction similar to **S21**. The inclusion of the Ni(II) metal center is one of the main driving forces between the differences seen in the NSD profiles of **S22** and **S23** aside from the break in aromaticity. There is a characteristically large *ruf* conformation that is common in the structures of Ni(II) macrocycles observed thus far. The chlorin **S23** has the largest D_{ip} observed in the fused chlorins up to this point as the largest *m-str* and *bre* conformations are observed in this structure. The NSD of **S23** shows slightly larger *sad*, *ruf*, *wav*(y) and *pro* normal deformations. The D_{ip} has also decreased and the main contribution to the *ip* distortion is the *bre* mode. The ring's conformation induces a large *ruf* configuration to alleviate the ring strain. There is also an equally significant *sad* configuration due to intermolecular short contacts in the packing system. A moderate *dom* contribution is reflective of the core hydrogen's pointing out of the plane of the macrocycle. A cyclohexanone fused to a chlorin macrocycle with an ester and five methyl groups also substituted onto the periphery creates the structure of **S24** (anhydrobonellin methyl ester, AHBONM).[45e] In comparison to **S22**, the D_{oop} of **S24** has increased by 0.456 Å. Even though there are fewer peripheral substituents on **S24** in comparison to **S22**, the increase in D_{oop} is a result of the completely reduced fused ring increasing the *oop* distortion modes. Conversely, the D_{ip} is 0.063 Å smaller than **S22** due to the reduced number of peripheral substituents which is characterized by a smaller *m-str* conformation observed in the NSD profile.

For the structures of **S25-S27**, the overall feature is derived by the fused ring attached to the pyrrole adjacent to the reduced pyrrole ring rather than in the previous structures where it is directly attached. In **S25** (OJOXIV),[45f] the polar iminopyranone fused to the free base chlorin generates a D_{oop} of 0.547 Å due to the moderate *sad* and large *ruf* conformations. In this structure, the fused ring is rather planar and does not

seem to excessively distort the macrocycle. It is clear that most of the macrocycle distortion comes from the β-substituted reduced pyrrole rings and its interactions with the cyclohexane solvent. Other artefacts in the crystal packing are the R^1 substituent is held co-planar to the fused ring resulting in a high degree of overlap with the macrocycle core. This forms a head-to-head overlap in the crystal packing which is complemented by head-to-head π-stacking between the unsubstituted pyrrole units. The D_{ip} of **S25** is slightly smaller than its D_{oop} (0.347 Å) and has meaningful *N-str* and *bre* configurations. A Zn(II) occupying the core of this chlorin (**S26**, OJOXUH)[45f] makes the macrocycle more non-planar and reduces *ip* distortion. The D_{oop} (0.898 Å) of this Zn(II) chlorin consists of a large *sad*, moderate *ruf*, *dom* and *pro* contributions. The reduced D_{ip} is due to smaller *N-str* and *bre* configurations, which is representative of the Zn(II) contracting the chlorin core due to the Zn(II)-N bonds. The only structural difference between **S27** (OJOXOB)[45f] and **S25** is that the R^1 substituent has a phenyl amine in **S27** replacing the benzyl amine in **S25**. These structural changes decrease the D_{oop} by 0.028 Å and the D_{ip} by 0.033 Å. The change in *sad* conformation in **S27** makes the macrocycle more planar whereas the smaller *N-str* contribution from the core intramolecular hydrogen bonding decreases the *ip* distortion. The main *oop* conformations observed in **S28** (PIRCIC) and **S29** (PIRCOI)[45g] are *sad*, *ruf* and *dom*. Their sole contribution to the *ip* distortion is the *bre* mode. The structures of **S28** and **S29** are an interesting example of how subtle changes to the conformation can result in significant changes to the NSD profiles. The D_{oop} of **S29** (0.760 Å) is almost double that of **S28** (0.406 Å). This is due to the looser packing of **S28** with the ester group point above the macrocycle plane and forming a shield for any π-stacking. Whereas **S29** shows a tight π-stacked structure as a result of having the ester group pointing above and below the macrocycle plane and giving rise to a higher *oop* distortion.

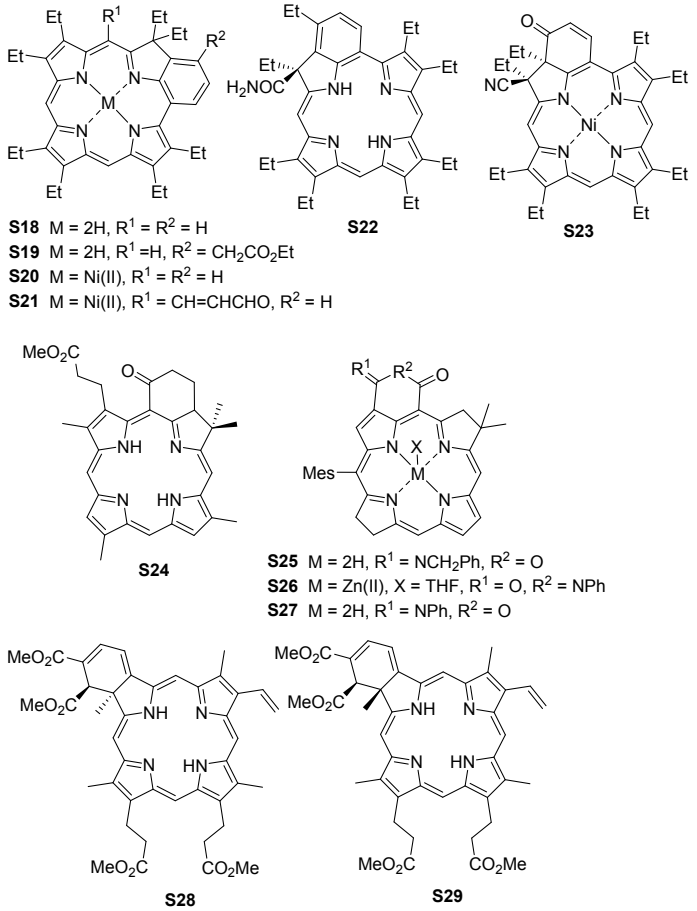

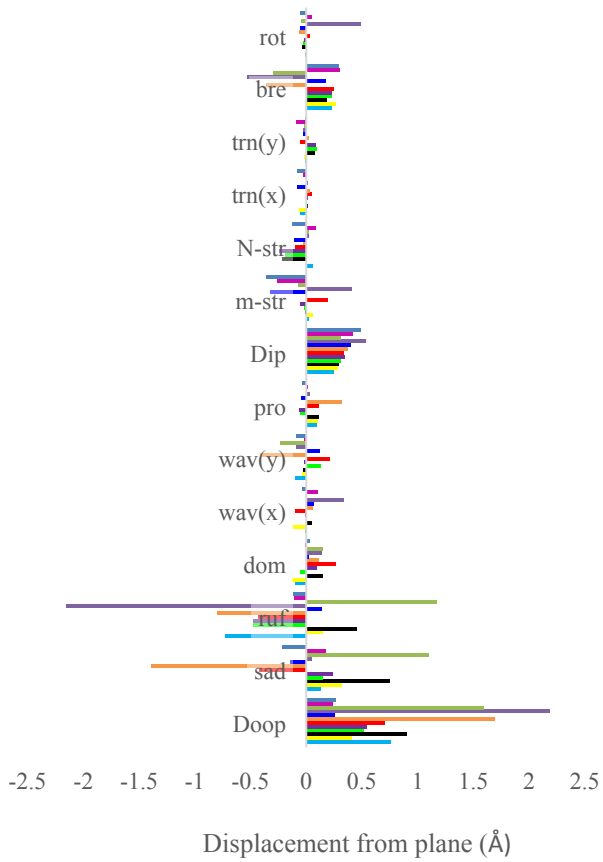

	Color	CCDC	Metal (M)	Axial ligand (X)	Solvent	Ref.
S18		JUNZIB	2H	–	–	43g
S19		QIRHEE	2H	–	–	45a
S20		OEBPNI	Ni(II)	–	–	45b
S21		VUFTEV	Ni(II)	–	–	45c
S22		XIXVAB	2H	–	–	45d
S23		XIXTUT	Ni(II)	-	–	45d
S24		AHBONM	2H	–	–	45e
S25		OJOXIV	2H	–	C_6H_{12}	45f
S26		OJOXUH	Zn(II)	THF	–	45f
S27		OJOXOB	2H	–	–	45f
S28		PIRCOI	2H	–	–	45g
S29		PIRCIC	2H	–	–	45g

Figure S18 Fused chlorins series and NSD analysis of the X-ray crystallographic structures observed in the fused chlorin compounds listed in the table. Table contains the color corresponding to the NSD graph, CCDC reference codes, metal in the core (M), axial ligand attached to the metal (X), and solvent in the respective unit cell.

The second group of fused chlorins is shown in Fig. S19. The fusing of a phthalimide species to a chlorin as well as the substitution of four methyl groups, two ester groups and a vinyl group (**S30**; NEZLOV),[46a] reduces the average *oop* distortion compared to **S28** and **S29**. The *ip* distortion has increased slightly in **S30** due to the moderate *m-str*, and large *N-str*, and *bre* distortion modes. The Ni(II) metal in the core of a quinolone oxide fused triphenylchlorin (**S31,** XUCBEE)[46b] generates large *ruf* conformations as previously seen. Additionally, the introduction of meso substituents increases the non-planarity of the structure due to *peri* interactions. The fused chlorin that has two rings fused to the macrocycle (**S32,** YAQXET)[46c] and has slightly increased non-planarity compared to the free base chlorin that has only one ring fused to it (**S30**). The cyclohexanone fused ring counteracts the ring strain caused by the fused aromatic ring resulting in only a slight increase in D_{oop} and D_{ip} distortion modes. The structures of **S33** (YACGOB)[46d] have *ruf* distortions due to the tetra-fluoro-chromene annulated fused ring. The independent molecules of the structure, **S33**, are all more non-planar than a phthalimide fused ring to the chlorin macrocycle (**S30**) due to the annulated fused ring as well as the sulfane's (**S33**) intermolecular interactions increasing the *ruf* character in the structure. The structures also have meaningful *oop* distortion from the rest of the modes bar the *sad*. There is less *ip* distortion in these structures due to a small *bre* configuration. The difference between the two independent molecules for compound **S33** results in different solvent interactions. Ring N1-N4 shows a hydrogen bond formed between the core nitrogen atoms and the CH_3SH solvent molecule were as ring N5-N8 there are no solvent interactions observed.

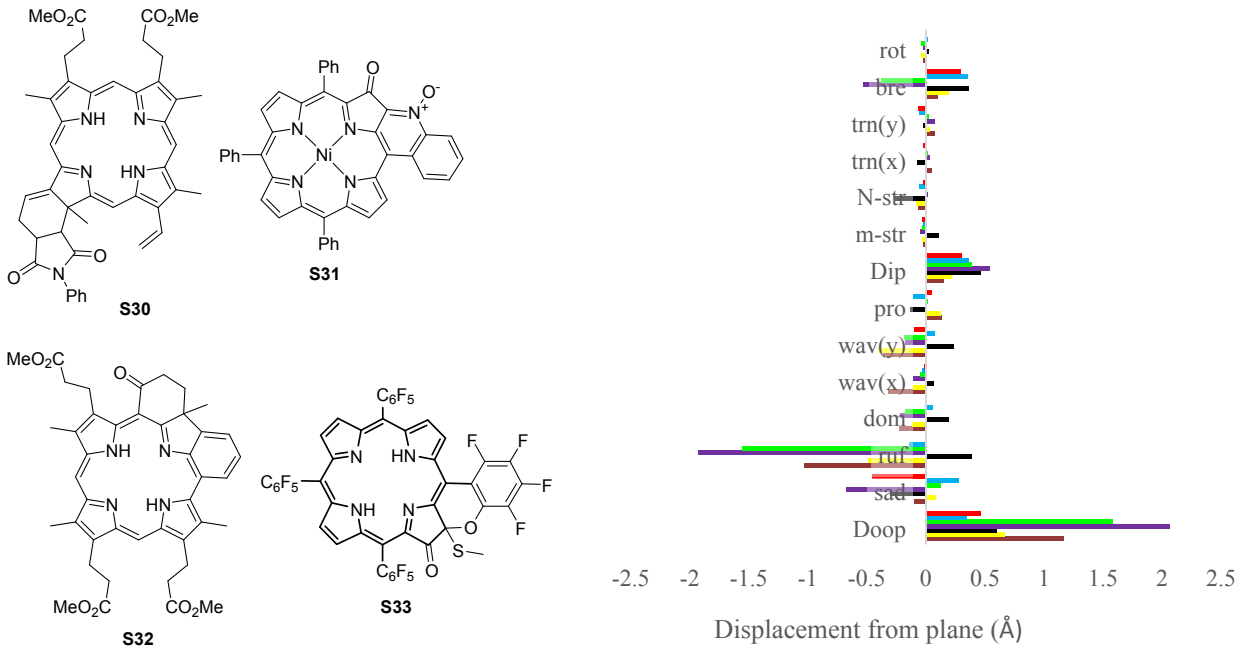

	Color	CCDC	Solvent	Ref.
S30[i]		NEZLOV (N1-N4 ring)	–	46a
S30[ii*]		NEZLOV (N5-N8 ring)	–	46a
S31[i]		XUCBEE (N1-N4 ring)	DCM, C_5H_{12}	46b
S31[ii]		XUCBEE (N5-N8 ring)	DCM, C_5H_{12}	46b
S32		YAQXET	–	46c
S33[i]		YACGOB (N1-N4 ring)	DCM, CH_3SH	46d
S33[ii]		YACGOB (N5-N8 ring)	DCM, CH_3SH	46d

Figure S19 Further fused-chlorins series and the NSD analysis of the X-ray crystallographic structures observed in the fused chlorin compounds listed in the table. Table contains the color corresponding to the NSD graph, CCDC reference codes, and the solvent in the respective unit cell.

Overall, the non-planarity of these fused β-substituted chlorins depends on the metal in the core and the peripheral substituent. The fused rings make the chlorin macrocycle more planar as well as inducing specific conformations based on the ring's nature.

2.4 Tetrahydroporphyrins (Bacteriochlorins and Isobacteriochlorins)

2.4.1 Free base bacteriochlorins

Fig. S20 compiles the free base bacteriochlorin structures studied.

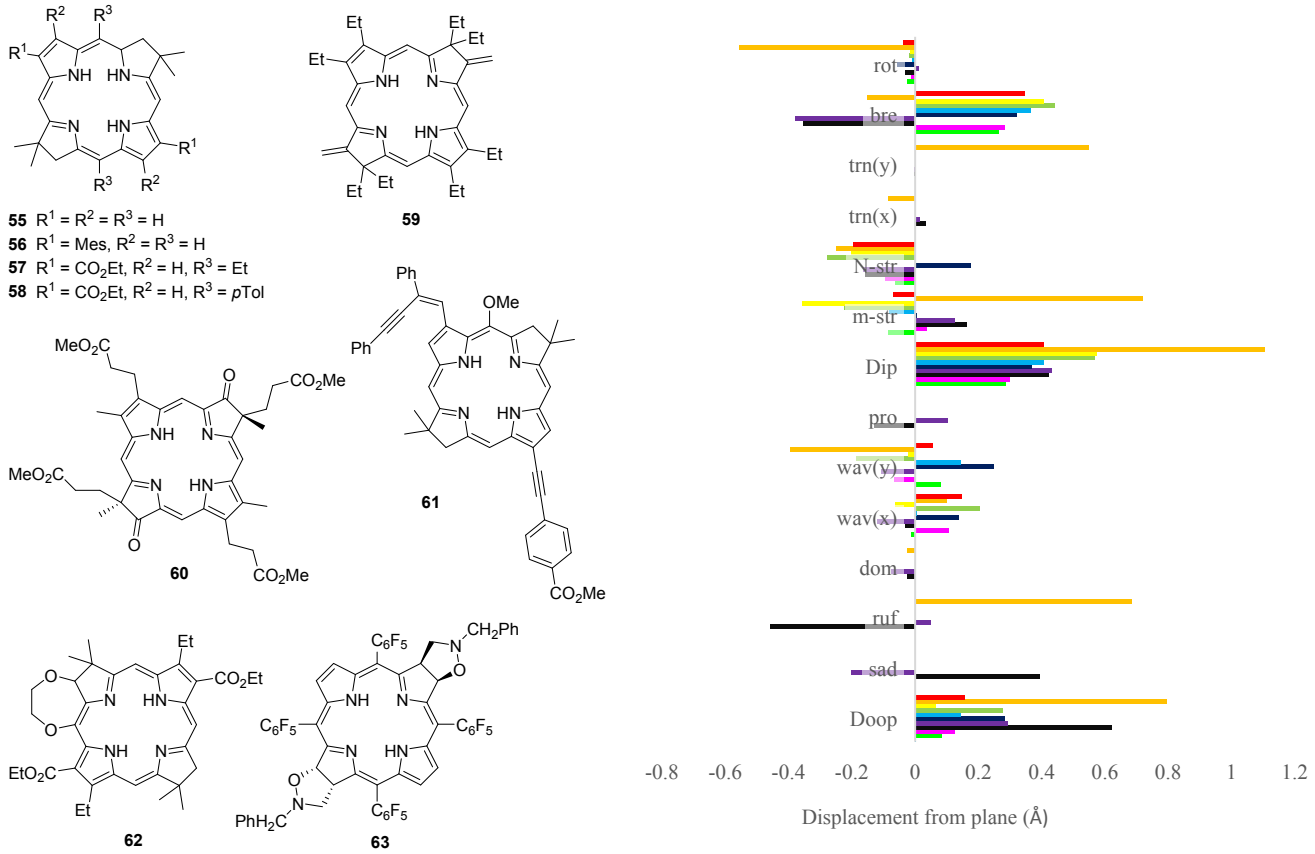

	Color	CCDC	Solvent	Ref.
55		BENROD	–	48a
56		BENRIX	–	48a
57		ECASUZ	–	48b
58		ECAFUM	–	48b
59		CONHIW	Hexane, DCM	48c
60		RIPMAE	–	48d
61		SUVBES	C_6H_{12}	48e
62		UYITIH	–	48f
63^{i}		BAGKIG	–	48g
63^{ii}		BAGKIG	–	48g

Figure S20 Free base bacteriochlorins series and the NSD analysis of the X-ray crystallographic structures observed in the free base bacteriochlorin compounds listed in the table. Table contains their CCDC reference codes, color corresponding to the NSD analysis, and solvent in the respective unit cell.

2.4.2 M(II) complexes of bacteriochlorins

The structures of the M(II) complexes of bacteriochlorins investigated in this section are shown in Fig. S21. The Cu(II) metal in the core of the bacteriochlorin **S34** (BENRET with four crystallographically independent molecules)[48a] greatly increases the D_{oop} compared to the most closely related free base structure (**55**) with the exception of **S34^{iv}.** The first independent molecule of **S34^{i}** has a substantial *ruf* conformation as well as significant *dom* and *pro* configurations. The rest of the molecules in BENRET, bar the exception already mentioned (**S34^{iv}**), have considerable *sad*, *dom* and *pro* conformations. To prove this, the average diagonal distance between the core nitrogen's of **S34**'s molecules and **58** were measured (Cu(II) vs free base bacteriochlorins, 4.01 Å vs 4.205 Å, respectively). All the average-cross diagonal nitrogen bond lengths were measured using the CCDC program, Mercury.[22] There is primarily *ruf* character in the 3D structure. There is also a significant *pro* conformation as well as a meaningful *sad* configuration. The displacement of the D_{oop} is 0.722 Å bigger than the D_{ip}. The main *ip* distortion mode is the *N-str* mode as a consequence of the short Cu(II)-Nitrogen bond narrowing the size of the macrocycle core. All of the independent molecules bar **S34^{iv}** have D_{oop} values of approximately 0.900 Å. The D_{oop} of **S34^{iv}** is 0.278 Å and like some, the majority of the free base bacteriochlorins, only have *wav*(x) and *wav*(y) contributions to the D_{oop}. The D_{ip} of this molecule is larger than the rest of the molecules in BENRET. There are significant *N-str* and *bre* configurations and there is considerable *oop* distortion due to intermolecular interactions as seen before. The presence of a Ni(II) metal in the center of the bacteriochlorin (**S35**, DEGTAK)[49] largely increases the D_{oop} by

approximately 1.000 Å. This is mainly due to the Ni(II) metal in the bacteriochlorins inducing a large *ruf* character to this overall structure. There is also a significant *bre* conformation which increases the D_{ip} compared to **S34**.

	Color	CCDC	Solvent	Ref.
S34[i]		BENRET	–	48a
S34[ii]		BENRET	–	48a
S34[iii]		BENRET	–	48a
S34[iv]		BENRET	–	48a
S35		DEGTAK	C_6H_6	49

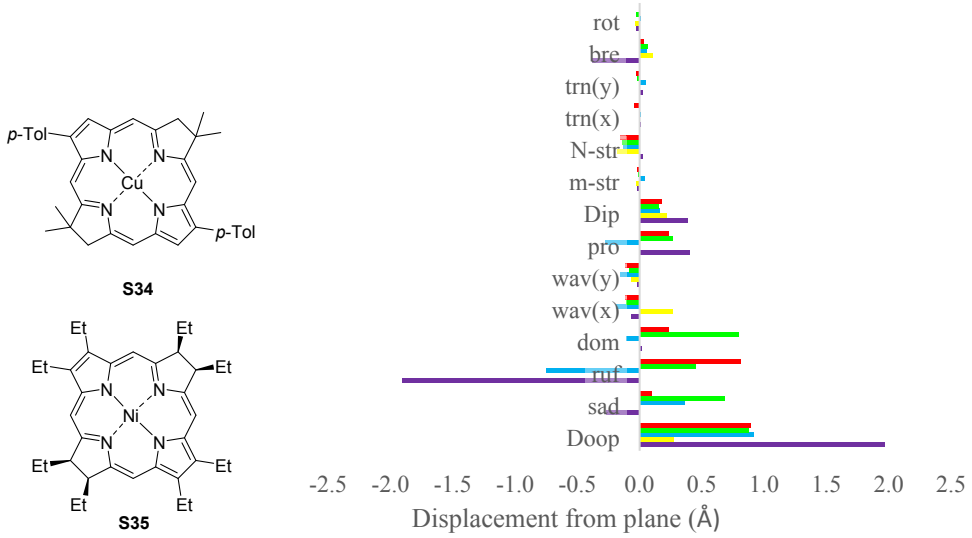

Figure S21 Metal bacteriochlorins series and the NSD analysis of the X-ray crystallographic structures observed in the metal bacteriochlorin compounds listed in the table. Table contains their CCDC reference codes, color corresponding to the NSD analysis, and solvent in the respective unit cell.

2.4.3 Free base isobacteriochlorins

The structure of the isobacteriochlorins investigated and a graphical representation of the NSD data are given in Fig. S22.

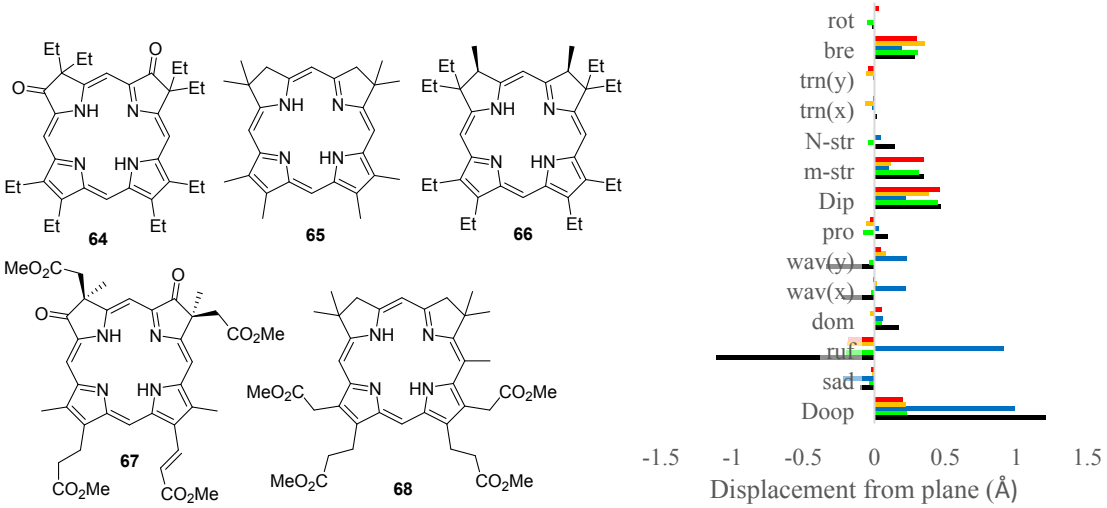

	Color	CCDC	Solvent	Ref.
64		SUCMIM	–	50a
65		BEYXEI	–	50b
66		BEJKEG	–	50c
67		KOSKEI	$CHCl_3$	50d
68		LEVXAL	–	50e

Figure S22 Free base isobacteriochlorins series and the NSD analysis of the X-ray crystallographic structures observed in the free base isobacteriochlorin compounds listed in the table. Table contains their CCDC reference codes, color corresponding to the NSD analysis, and solvent in the respective unit cell.

2.4.4 M(II) isobacteriochlorin complexes

The structure of the isobacteriochlorins investigated and a graphical representation of the NSD data are given in Fig. S23.

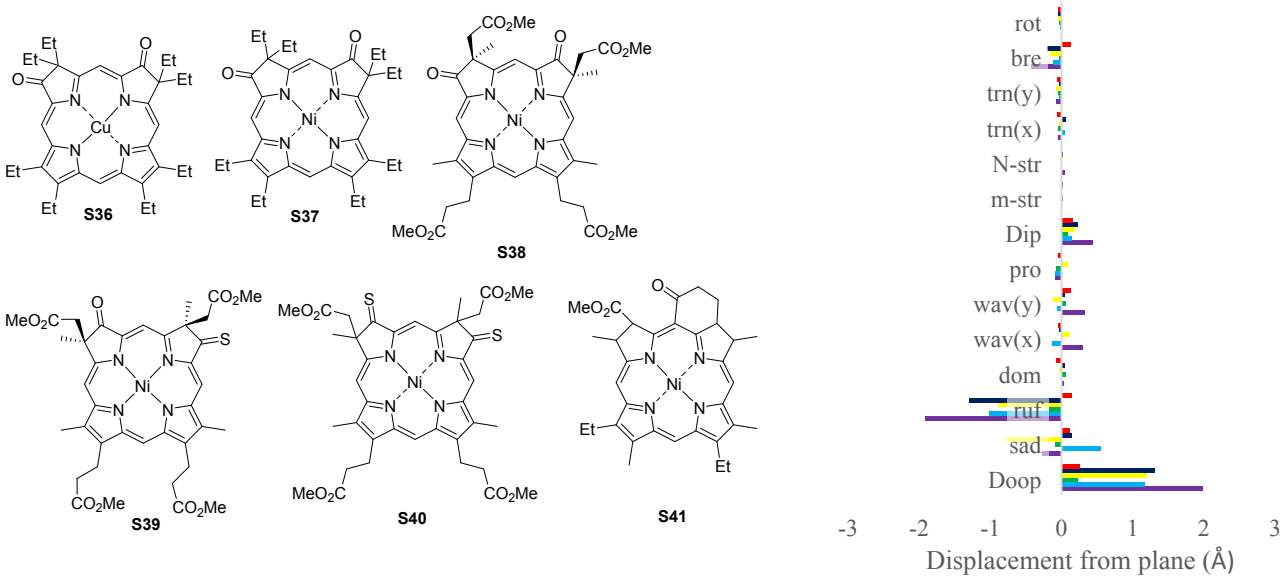

	Color	CCDC	Solvent	Ref.
S36		DOMKOF	DCE	51a
S37		PETHEB	–	43d
S38		VARFUP	–	51b
S39		SOXWUZ	$CHCl_3$	51c
S40		SOXWOT	H_2O	51c
S41		KODHAM	–	51d

Figure S23 Metal(II) isobacteriochlorins series and the NSD analysis of the X-ray crystallographic structures observed in the metal(II) isobacteriochlorin compounds listed in the table. Table contains their CCDC reference codes, color corresponding to the NSD analysis, and solvent in the respective unit cell.

These metallated isobacteriochlorins (IBCs) have D_{oop} content in the range of 0.234–1.986 Å and a D_{ip} range of 0.086–0.444 Å. The Cu(II) and Ni(II) IBCs can be directly compared with a free base IBC *via* the contrast of **64**, **S36** (DOMKOF)[51a] and **S37** (PETHEB).[43d] These structures have identical peripheral substituents and only differ by the presence or absence of a metal in the core. In the crystal structure, this is represented by a shift from the π-stacking seen in the structure of **64** towards the face-to-edge packing seen in **S36** and **S37**. The residence of a Cu(II) metal in the center of the bacteriochlorin (**S36**) slightly increases the D_{oop}, whereas a Ni(II) metal (**S37**) drastically increases the D_{oop} compared to the free base derivative (**64**), as seen previously in the section throughout. **S36** exists in a 3D structure that possesses moderate *sad*, *ruf* and *wav*(y) *oop* conformations, whereas **S37** contains mainly *ruf* character with a relatively small amount of *sad* character. The D_{ip} of **64** is more than twice the value than that of **S36** and **S37**, with the latter being slightly more distorted. Both **S36** and **S37** contain solely a *bre* conformation and conversely, **64** contains a large *m-str* and *bre* contribution to the *ip*. Contrasting the NSD of these two compounds (**S36** and **S37**), the contributions from the *ruf* decreases yet the *sad* increases. The D_{ip} declines by 0.030 Å as represented by the smaller *bre* conformation. The structural reason for the decline in *oop* distortion is due to the esters lying in the plane of the macrocycle and reducing the possible non-planarity. Previously in the bacteriopheophorbide-related compounds above, the ester generally causes the macrocycle to be non-planar. Looking into the structural differences between **S37** and **S38** (VARFUP),[51b] the substitution of four ester groups and two oxo groups onto the periphery occurs and this slightly lessens the D_{oop} and the D_{ip}. In the crystal structure of **S38,** it is clear that the ester groups on the reduced pyrrole side of the macrocycle point above the macrocycle while the ester groups on the opposite side of the macrocycle point below the plane. This allows for a significant overlapped structure to form in the crystal packing and this indicates that the ester in **S38** causes the isobacteriochlorin macrocycle to be planar. Switching one of the oxo groups in **S38** for a sulfur affords the structure of **S39** (SOXWUZ)[51c] and significantly reduces the D_{oop} by 0.964 Å and the D_{ip} by 0.109 Å. In the crystal packing, this is represented as a tightly packed π-stacking head-to-tail pattern with the sulfur moiety now interacting with the $CHCl_3$ solvent. There are no significant contributions to the D_{oop} of **S39** apart from a moderate *ruf* configuration and there is no meaningful contribution to the *ip* distortion. The rise in D_{oop} is a result of the large *sad* and *ruf* contributions as well as the moderate *wav*(x) conformation. The increasing *ip* distortion is mainly because of the rise in *bre* contribution to the *ip* distortion. This contribution as well as meaningful *sad*, *wav*(x) and *wav*(y) conformations are the main *oop* contributions. When the last oxo moiety is replaced in **S39** by a sulfur, the structure of **S40** (SOXWOT)[51c] is generated. The introduction of this second sulfur atom significantly increases the D_{oop} by 0.939 Å whereas the D_{ip} rises slightly by 0.055 Å. This second sulfur atom, while itself being only a moderate adjustment of the macrocycle, is seen to act as a pseudo axial ligand to the Ni(II) metal center of **S40**. Thus, directly affecting the distortion of the macrocycle as represented by an increase in the *ruf* distortion mode. The fused cyclohexanone ring in **S41** (KODHAM),[51d] forces the adjacent pyrrole to be severely distorted in a *ruf* conformation. This ring, as well as the two ethyl, four methyl and ester groups, make up the structure of **S41**. The D_{oop} of **S41** is 0.813 Å larger than that of **S40** and the D_{ip} is 0.303 Å larger than the D_{ip} of **S40**. The D_{ip} of **S41** obtains its distortion mainly from the *bre* configuration. Overall, this series demonstrates how the introduction of a metal(II) center into the core of an isobacteriochlorin can affect the overall conformation based off the type of metal used and how it interacts with the environment of the peripheral substituents.

2.5 Manipulation of the phytochlorin skeleton

From a more biological point of view, there are many known natural drastic changes observed in the conformation of the phytochlorin skeleton. However, only the most common and well known structurally related compounds were studied and their NSD profiles discussed. These include the structures with the CCDC reference codes listed in the table below (Fig. S24).

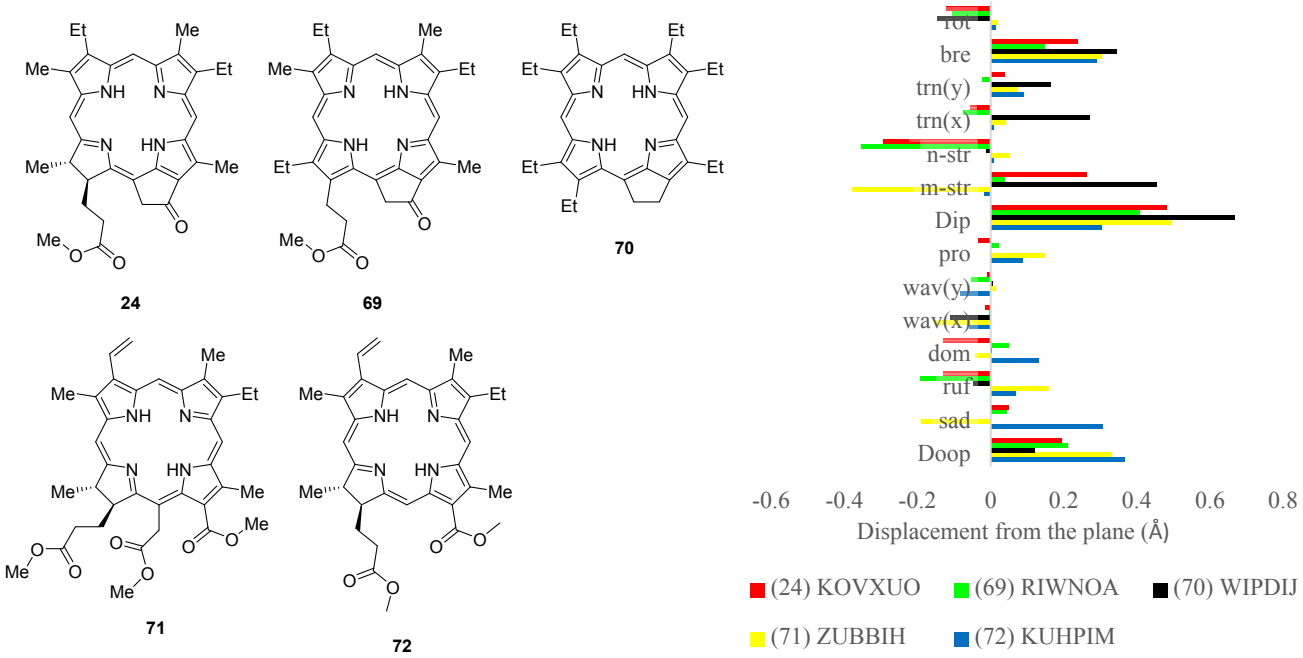

	CCDC	Color	References
24	KOVXUO		34b
69	RIWNOA		34a
70	WIPDIJ		52a
71	ZUBBIH		52b
72	KUHPIM		52c

Figure S24 Phytochlorin related biological compound series and the NSD analysis of the X-ray crystallographic structures observed in the phytochlorin related biological compounds listed in the table. Table contains their CCDC reference codes, color corresponding to the NSD analysis, and solvent in the respective unit cell.

In the phytochlorin methyl ester structure of KOVXUO (**24**),[34b] the D_{oop} arises from the significant *ruf* and *dom* modes of distortion. This D_{oop} is due to the ester induced *ruf* distortion and the meaningful *dom* configuration. These *ruf* and *dom* contributions are artefacts of the intermolecular interactions seen in the packing modes of this structure. On one side of the macrocycle plane, the ester groups interact with the core pulling the N···H amines out of the macrocycle plane, but the other side is shielded from the ester groups due to a π-stacking system. This π-system is instigated by an edge-on interaction between the oxo moiety and the meso hydrogen atoms creating a sheet like system of hydrogen-bonding. The ester interacting with the core of the tetrapyrrole is responsible the for large *N-str ip* distortion. This mode, as well as the large *m-str* and *bre* distortions, are the reason for the higher *ip* displacement than *oop* displacement. The *m-str* distortion is predominant because of the oxo moiety and meso hydrogen short contacts in the packing system. The phytoporphyrin methyl ester structure of RIWNOA (**69**)[34a] has the third highest D_{oop} in this series due to it having the largest *ruf* contribution. This, however, is not only due to the presence of the ester but due to the pyrrole trans to the ester. This "trans pyrrole" has a methyl and ester group at the β-positions and exhibit a *ruf* type conformation. This 3D conformation, the ester induced *ruf* conformation, and the ester's non-classical intermolecular hydrogen bonding with the carbonyl oxygen, all give rise to the *oop* distortion. In the crystal packing, this is revealed through a high π-stacking with a head-to-tail overlap. This structure has the second lowest *ip* distortion, however it is still larger than any *oop* distortion's displacement (The D_{ip} is almost twice the displacement of its own D_{oop}). The closest phorbine relate structure in the CCDC, WIPDIJ (**70**),[52a] has the lowest *oop* distortion and highest *ip* distortion in this series. This can be explained by the head-to-tail packing observed and the main contacts are non-classical intermolecular hydrogen bonds between the peripheral alkyl groups. This also explains the small *ruf* contribution to the non-planarity as well as *wav*(x) contributing the most *oop* character to the 3D structure. This crystal structure has the largest *ip* distortion in this series due to the large contributions from all the modes bar the *N-str* mode. The chlorin e_6 trimethyl ester structure, ZUBBIH (**71**),[52b] obtains its *oop* character from all distortion modes, bar *wav*(y) and *dom*. It has significant *sad* and *ruf* distortions due to the presence of *peri*-interactions from the esters and the esters giving rise to *ruf* configurations. These esters are also the reason for the largest *m-str* configuration observed in the NSD profile in Fig. S28. In the crystal packing, this is represented by a loose head-to-head π-stacked structure with the ester groups interacting with the inner core system on one side of the macrocycle plane. The closest rhodochlorin derivative in the CCDC, KUHPIM (**72**),[52c] has the largest D_{oop} and the smallest D_{ip} in this series. This is the only crystal structure that has a larger *oop* displacement than *ip* displacement. The

large D_{oop} arises from significant contributions from all distortion modes, the sad mode contributing the largest amount of *oop* character. This arises due to the ester interacting with the peripheral ethyl groups.

Overall in this series, there is larger *ip* distortion than *oop* distortion in these crystal structures, as seen in the bacteriopheophorbide related structures. The D_{ip} is in the range of 0.3045–0.6685 Å and the D_{oop} ranges from 0.1202–0.3661 Å. These free base tetrapyrroles have larger *ip* distortion due to favorable intermolecular interactions.

2.6 Complete NSD conformation analysis tables of the compounds studied

Table S1: NSD. Full details of NSD conformation analysis of the compounds studied [Å].

					Out-of-plane distortions							In-plane distortions								
#	Compound	M	CSD #	Ref	D_{oop}	□$_{oop}$	B_{2u}	B_{1u}	A_{2u}	$E_{g(x)}$	$E_{g(y)}$	A_{1u}	D_{ip}	□$_{ip}$	B_{2g}	B_{1g}	$E_{u(x)}$	$E_{u(y)}$	A_{1g}	A_{2g}
Test cases – free base compounds																				
5,10,15,20-Tetraphenylporphyrin																				
6a	5,10,15,20-Tetraphenylporphyrin bis(benzaldehyde) clathrate	2H	JIVRAH	25a	0.0146	0.0076	0	0	0	-0.0115	0.009	0	0.2006	0.0158	0.0396	-0.0167	0	0	0.1959	-0.0026
6b	5,10,15,20-Tetraphenylporphyrin bis(*m*-xylene) clathrate	2H	SEMNIH	25b	0.0389	0.009	0	0	0	0.0389	-0.0026	0	0.1765	0.0118	-0.056	0.0496	0	0	0.1577	0.0261
6c	5,10,15,20-Tetraphenylporphyrin bis(*m*-xylene) clathrate	2H	SEMNIH01	25c	0.0373	0.0033	0.0001	0.0003	-0.0001	-0.0009	-0.0372	0.0001	0.2109	0.013	-0.0542	0.004	-0.0001	0.0007	0.2038	0.0012
6d	5,10,15,20-Tetraphenylporphyrin	2H	TPHPOR01	25d	0.258	0.0355	0	0	0	-0.2314	0.1142	0	0.196	0.0185	0.015	0.0482	0	0	0.1883	0.0201
6e	5,10,15,20-Tetraphenylporphyrin	2H	TPHPOR04	25f	0.2668	0.0371	-0.0001	-0.0002	-0.0001	0.2406	-0.1151	0.0002	0.208	0.0215	0.0323	0.0519	-0.0002	0	0.198	0.0183
6f	5,10,15,20-Tetraphenylporphyrin	2H	TPHPOR11	25g	0.2663	0.0399	-0.0004	-0.0004	0	0.2507	-0.0898	0.0002	0.2357	0.0251	0.0393	0.0521	-0.0003	-0.0006	0.2255	0.0215
6g	5,10,15,20-Tetraphenylporphyrine	2H	TPHPOR12	25h	0.2248	0.0379	0.0003	-0.0002	-0.0001	0.2071	-0.0876	0.0003	0.1803	0.0186	0.021	0.0487	-0.0007	0.0006	0.1721	0.0083
6h	5,10,15,20-Tetraphenylporphyrin	2H	TPHPOR13	25i	0.2691	0.0399	-0.0001	0.0003	-0.0003	-0.2525	0.093	-0.0006	0.2266	0.0238	0.0385	0.053	0.0001	-0.0004	0.2156	0.0238
6i	5,10,15,20-Tetraphenylporphyrin	2H	TPHPOR14	25j	0.262	0.0361	0.0003	0.0004	-0.0005	-0.238	-0.1095	0.0002	0.2027	0.0223	-0.0143	0.0338	0.0002	0.0006	0.1979	-0.0239
6j	5,10,15,20-Tetraphenylporhyrin anthracene clathrate	2H	XAGLOG	25k	0.218	0.0159	0.0005	-0.0004	-0.0002	0.1285	0.1761	0	0.2026	0.0201	0.0362	-0.0423	0.0003	0.0002	0.1948	0.0016
6k	5,10,15,20-Tetraphenylporphyrin phenanthrene clathrate	2H	XAGMAT	25l	0.2582	0.0259	-0.0008	-0.0003	0.0003	0.1432	0.2149	0.0004	0.1969	0.0149	0.0146	0.0333	0.0003	-0.0001	0.1935	-0.0047
2,3,7,8,12,13,17,18-Octaethylporphyrin																				
7a	2,3,7,8,12,13,17,18-Octaethylporphyrin	2H	OETPOR10	26a	0.1095	0.0113	0	0	0	-0.063	0.0895	0	0.2279	0.0183	0.0016	-0.058	0	0	0.2204	0.0001
7b	2,3,7,8,12,13,17,18-Octaethylporphyrin 7,7,8,8-tetracyanoquinodimethane clathrate	2H	OKOQUA	26b	0.0933	0.0055	0.0001	0.0009	0.0004	-0.0176	-0.0917	-0.0001	0.3262	0.0109	0.2327	-0.0099	0.0002	0	0.2283	-0.0064
XEtTPP series																				
8	2,3-Diethyl-5,10,15,20-tetraphenylporphyrin	2H	TATPOT01	27b	0.6164	0.0088	-0.5955	-0.0552	0.0443	0.0307	-0.1374	0.0223	0.3458	0.0283	0.056	0.2424	-0.0475	0.0018	0.2354	-0.0056
9	2,3,12,13-Tetraethyl-5,10,15,20-tetraphenylporphyrin dichloromethane solvate	2H	TATPUZ01	27b	1.8137	0.0376	-1.8118	-0.0398	0.0614	-0.0075	-0.0396	0.0075	0.268	0.0377	-0.0015	0.2658	-0.0041	0.0138	0.0309	-0.0028
10	2,3,7,8-Tetraethyl-5,10,15,20-tetraphenylporphyrin methanol solvate	2H	TATQAG01	27b	2.3542	0.054	2.2852	-0.2476	0.0358	-0.2502	0.4398	-0.0334	0.1369	0.0611	-0.0072	0.0752	-0.0424	0.0216	-0.0973	-0.0361
11	2,3,7,8,12,13-Hexaethyl-5,10,15,20-tetraphenylporphyrin dichloromethane solvate	2H	TATQEK01	27b	2.8466	0.0498	2.8231	0.1686	0.0008	0.1449	0.289	-0.0259	0.3753	0.0727	-0.0422	0.2340	-0.0068	0.0167	-0.2898	-0.0041
12	2,3,7,8,12,13,17,18-Octaethyl-5,10,15,20-tetraphenylporphyrin ethanol solvate	2H	SATQOU	27c	3.46	0.069	-3.4555	-0.099	0.0337	0.0997	0.1026	0.0096	0.5151	0.1049	0.0565	-0.0896	0.0365	-0.0391	-0.5012	-0.0026
12a	2,3,7,8,12,13,17,18-Octaethyl-5,10,15,20-tetraphenylporphyrin bis(dichloromethane) clathrate	2H	QAWFIE	27c	3.9489	0.177	-3.6587	-1.4811	0.1127	0	0	-0.0301	1.0546	0.1751	-0.0942	-0.1978	0	-0.0005	-0.954	0.3924
XEtTPC series																				
13	7,8-Diethyl-5,10,15,20-tetraphenylchlorin	2H	GELGUZ	28	1.1536	0.0251	-1.103	-0.2781	0.0443	0.0856	-0.1647	0.0177	0.2932	0.0344	-0.0458	-0.1062	-0.0574	-0.0573	0.2568	-0.0086
14	12,13-Diethyl-5,10,15,20-tetraphenylchlorin	2H	GELJEM	28	1.9501	0.0245	1.8972	-0.3766	0.0091	0.2393	-0.0182	0.0636	0.277	0.0421	0.0019	0.2638	-0.0623	-0.0102	0.056	-0.0039
15	2,3,7,8-Tetraethyl-5,10,15,20-tetraphenylchlorin•CH_2Cl_2•CH_3OH	2H	GELQAP	28	1.8666	0.0381	-1.7541	-0.503	0.1185	0.2167	-0.2773	0.1289	0.1931	0.0457	0.1427	-0.0732	-0.0624	-0.0289	0.0744	-0.0361
16	7,8,12,13-Tetraethyl-5,10,15,20-tetraphenylchlorin	2H	GELHAG	28	2.7391	0.04	-2.6645	-0.4588	-0.11	-0.2868	-0.3127	-0.0103	0.1949	0.0663	-0.0335	0.0924	-0.0208	0.0611	-0.1551	0.0096
Test cases – metal complexes																				
5,10,15,20-Tetraphenylporphyrins and 2,3,7,8,12,13,17,18-octaethylporphyrins																				
Zn6a	(5,10,15,20-Tetraphenylporphyrinato)zinc(II)	Zn(II)	ZZZTAY02	30	0.2368	0.0310	0	0	0	-0.1939	0.1359	0	0.1480	0.0093	0.0136	0.0226	0	0	0.1451	0.0126
Zn6b	(5,10,15,20-Tetraphenylporphyrinato)zinc(II)	Zn(II)	ZZZTAY03	32	0.1593	0.0115	0	0	0	-0.1583	0.0179	0	0.1522	0.0081	-0.0028	0.0105	0	0	0.1518	0.0008
Zn7a	(2,3,7,8,12,13,17,18-Octaethylporphyrinato)zinc(II)	Zn(II)	ALOKOB	31a	0.1658	0.0061	0.0001	0	0.0002	-0.1576	-0.0517	0.0001	0.1444	0.0095	0.0019	-0.0083	0	-0.0001	0.1441	-0.0003
Zn7b	(2,3,7,8,12,13,17,18-Octaethylporphyrinato)zinc(II) hemikis(7,7,8,8-tetracyanoquinodimethane)	Zn(II)	OKOREL	26b	0.3744	0.0076	-0.3183	-0.0763	-0.1007	0.1273	0.0782	0.0156	0.1465	0.0085	-0.0034	0.0027	-0.0053	-0.0146	0.1456	0.0033
XEtTPPs and XEtTPCs																				
Zn8	3-Picoline(2,3-diethyl-5,10,15,20-tetraphenylporphyrinato)zinc(II)	Zn(II)	RUTNEZ	27b	1.0543	0.0228	0.8957	0.4732	0.1616	-0.1868	0.1558	-0.0098	0.2151	0.0179	-0.0284	0.1698	-0.0274	0.0092	0.1244	0.0173
Zn9	Pyridine(2,3,12,13-tetraethyl-5,10,15,20-tetraphenylporphyrinato)zinc(II) hydrate	Zn(II)	RUTQAY	27b	1.7038	0.0383	1.5998	-0.5617	0.0215	0.1616	0.0217	-0.0318	0.2086	0.0273	0.0303	0.1925	-0.0156	-0.0302	0.0601	-0.0276
Zn11	(2,3,7,8,12,13-Hexaethyl-5,10,15,20-tetraphenylporphyrinato)zinc(II)	Zn(II)	RUTRAZ	27b	2.761	0.0422	-2.7218	-0.3307	0.2131	0.0014	-0.2446	0.0114	0.2534	0.0583	0.0405	0.0175	0.0067	-0.0084	-0.2490	0.0113
Zn12	Methanol(2,3,7,8,12,13,17,18-octaethyl-5,10,15,20-tetraphenylporphinato)zinc(II) methanol solvate	Zn(II)	JICNIS	31b	3.252	0.0676	-3.2477	0.1176	0.0373	-0.1042	-0.0383	-0.0019	0.3933	0.0864	0.0373	-0.0122	-0.0474	0.0136	-0.3882	0.0019
Zn13	(7,8-Diethyl-5,10,15,20-tetraphenylchlorinato)zinc(II)•CH_2Cl_2	Zn(II)	GELJAI	28	2.1513	0.0348	-2.1053	0.4205	0.0173	-0.0625	-0.1107	-0.0513	0.1056	0.0406	-0.021	-0.0141	-0.0776	-0.0444	-0.0495	-0.0094
Zn13a	(7,8-Diethyl-5,10,15,20-tetraphenylchlorinato)zinc(II)•MeOH	Zn(II)	GELQET	28	0.299	0.0153	0.2451	-0.0708	-0.1475	0.0149	-0.0447	0.018	0.2959	0.0217	0.0144	-0.0569	-0.0569	-0.0613	0.2776	0.0058
Zn17	Methanol(7,8,17,18-tetraethyl-5,10,15,20-tetraphenylchlorinato)zinc(II)•CH_2Cl_2•CH_3OH	Zn(II)	GELPIW	28	1.6573	0.0336	-1.6558	0	-0.0719	0	0	0	0.2731	0.0221	0	0.2454	-0.0001	0	0.1196	0
"Chlorophyll derivatives" = Phytochlorins																				
Free base phytochlorins																				
17a	Methyl pheophorbide a	2H	MPOPHA	33a	0.2541	0.0263	-0.1818	-0.0094	-0.0962	-0.0914	0.0242	0.1151	0.4611	0.0521	0.2724	-0.2844	-0.0817	0.0257	0.2013	-0.0983
17b	"	2H	MPOPHA02	33b	0.2461	0.0274	0.1851	0.0199	0.0884	0.0899	0.0151	0.099	0.5441	0.0695	-0.2568	-0.3779	-0.1095	-0.1031	0.2324	0.1031
17c	"	2H	MPOPHA03	33c	0.2386	0.0291	0.1733	-0.0122	0.0969	0.0844	-0.0283	-0.0972	0.448	0.0533	0.2511	-0.2927	-0.0923	0.0256	0.1741	-0.112
18	Ethyl pheophorbide b	2H	ROFVUE	33d	0.2006	0.0172	-0.1197	-0.0429	-0.0002	-0.1237	-0.0533	-0.0769	0.4949	0.0568	-0.3167	-0.2602	-0.0999	-0.0284	0.2364	0.1014
19	Methyl [4,5-Diethyl]-bacteriopheophorbide d (mol. 1 N1-N4)	2H	BIPBOR	33e	0.4316	0.0304	-0.2086	-0.1963	-0.1118	0.1746	-0.1823	-0.1674	0.4534	0.0676	0.1006	-0.3493	-0.0108	0.0584	0.2415	-0.1078
"	" (mol. 2 N5-N8)	2H	"	"	0.3332	0.0567	0.1991	-0.0883	0.0984	0.15	0.0714	-0.1622	0.4304	0.0493	0.1144	-0.3319	-0.0706	0.0275	0.2089	-0.1123
20	Methyl [12-acetyl-8-ethyl]-bacteriopheophorbide d	2H	SOSZOP	33f	0.3694	0.0373	-0.1197	-0.1657	0.0422	-0.0788	-0.2841	-0.0776	0.3898	0.0536	0.1136	-0.2931	-0.0602	-0.0067	0.2003	-0.0966
21	Methyl [4-isobutyl-5-ethyl]-bacteriopheophorbide d (mol. 1 N1-N4)	2H	BIPBIL	33e	0.4346	0.0409	-0.1027	-0.3503	-0.0765	0.1281	-0.0639	-0.1711	0.4584	0.0517	0.1981	-0.3276	-0.0583	0.032	0.2156	-0.1122
"	" (mol. 2 N5-N8)	2H	BIPBIL	"	0.4215	0.05	0.2139	-0.1532	0.1003	0.233	-0.0703	-0.1979	0.3786	0.0533	0.1091	-0.2807	-0.0697	-0.0275	0.2019	-0.079
22	Methyl [8-neopentyl,12-ethyl]-bacteriopheophorbide d	2H	BIXREF01	33g	0.467	0.0099	0.0654	0.0092	0.4372	-0.0245	-0.1473	-0.0166	0.4976	0.0538	0.2462	-0.3142	-0.0997	0.0371	0.2604	-0.0956
23	17-Decarboxyethyl-13^1-deoxo-17-propylphytochlorin (mol.1 N5-N8 ring)	2H	RIWNIU	34a	0.4096	0.0215	0.2748	0.2378	0.0862	-0.1071	-0.1072	0.0732	0.4968	0.054	0.1944	-0.3217	-0.0955	0.0206	0.2889	-0.1117
"	" (mol. 2 N1-N4)	2H	"	"	0.1865	0.0235	0.014	0.0108	0.0635	-0.0419	-0.1246	0.1146	0.5308	0.0525	0.3141	-0.2903	-0.1007	0.0183	0.2743	-0.1145
24	Methyl phytochlorin	2H	KOVXUO	34b	0.1937	0.02	0.0489	-0.1291	-0.1302	-0.014	-0.0089	-0.0353	0.4816	0.0541	0.2639	-0.2931	-0.0557	0.0388	0.2388	-0.1216
25	Methyl 3-deethyl-3-(4,4,4-trifluoro-1-hydroxy-3-oxo-but-1-en-1-yl)phytochlorin enol	2H	PEPJUR	34c	0.1716	0.0112	-0.0841	0.0795	0.0347	-0.0339	-0.1169	-0.005	0.5372	0.0591	0.2698	-0.2905	-0.1045	0.0391	0.3313	-0.096
Metallophytochlorins																				
Chlorophyllides																				

26	(H_2O)(Methyl pyrochlorophyllide a)magnesium(II)•Et_2O	Mg(II)	MPCHLM10	35a	0.173	0.0277	-0.0827	0.0297	0.0613	0.0754	0.0195	0.1113	0.3636	0.0571	0.1132	-0.2195	-0.0371	-0.0391	0.2523	-0.0684
27	(H_2O)(Methyl chlorophyllide a)•H_2O	Mg(II)	MCLPHD10	35b	0.2576	0.0107	0.1879	-0.0031	0.1292	-0.0487	-0.1079	0.0179	0.3571	0.0462	0.0405	-0.2261	-0.0829	0.0447	0.2289	-0.1163
28a	(H_2O)(Ethyl chlorophyllide a)•H_2O	Mg(II)	AECLPA01	35c	0.3265	0.0231	0.1755	0.1318	-0.1249	-0.1068	-0.1621	0.0719	0.3566	0.0473	0.0695	-0.2251	-0.067	0.0246	0.237	-0.1018
28b	(H_2O)(Ethyl chlorophyllide a)•H_2O	Mg(II)	AECLPA10	35e	0.331	0.0248	0.1838	0.1252	-0.11	-0.1115	-0.1739	0.0729	0.3745	0.0497	0.0878	-0.2467	-0.0717	0.0203	0.2372	-0.0992
29	(H_2O)(Ethyl chlorophyllide b)•H_2O	Mg(II)	ECPHBH	35d	0.3268	0.0217	0.2312	0.0485	-0.0859	-0.1387	-0.1483	0.0494	0.3729	0.052	0.1083	-0.2367	-0.0881	0.0376	0.2281	-0.1008
Other metallophytochlorins																				
30	[(Methyl 3-deethyl,3-carboximino-phytochlorinato)zinc(II)]$_n$•n$CHCl_3$ (cateana-□$^{\square}$-13^1-O…Zn polymer)	Zn(II)	CELRIU	36a	0.6362	0.0395	-0.5434	0.2619	0.0974	-0.0383	0.1141	0.1297	0.4165	0.0458	-0.0277	-0.3536	0.1015	0.0227	0.1681	0.0929
31	[Methyl 3^1-oxophytochlorinato)zinc(II)]$_n$•nCH_2Cl_2 (catena-□^{2}-17^3-oxo…Zn polymer)	Zn(II)	MEHGUD	36b	0.4673	0.0096	-0.4322	0.1054	-0.1108	-0.0523	0.0742	-0.0028	0.351	0.0502	0.0514	-0.2407	-0.0846	0.0174	0.2184	-0.0868
32	[Methyl 3-deethyl-3-((4-(pyridin-3-yl)phenyl)ethynyl)phytochlorinato]zinc(II) [catena-(μ-zinc-pyridin polymer] (mol. 1 N1-N5)	Zn(II)	XOKGOV	36c	0.3207	0.0281	0.0070	0.2587	0.0611	0.1599	0.0282	0.0757	0.4334	0.0451	0.0866	-0.3260	0.0586	-0.0024	0.2412	-0.1115
"	" (mol. 2, N6-N10)	Zn(II)	"	"	0.2786	0.045	0.1542	0.0551	-0.0132	0.165	0.0509	0.1444	0.3941	0.0431	0.0374	-0.3028	0.1041	0.0369	0.2084	-0.0811
33	[(Methyl 3^1,3^2-didehydro-3^2-(4-pyridyl)phytochlorinato)zinc(II)]$_n$•0.5nC_2H_3N (catena-μ^2-pyridyl-N…Zn polymer)(mol. 1, N1-N4)	Zn(II)	MIBJEO	36d	0.1755	0.0337	-0.0898	0.0868	-0.0508	-0.0246	-0.0538	-0.0956	0.4243	0.0511	0.005	0.3222	0.0154	0.0537	0.2527	0.096
"	" (mol. 2, N5-N8)	Zn(II)	"	"	0.5712	0.0404	0.3788	-0.306	-0.1816	-0.0056	-0.1208	0.2037	0.3427	0.0528	-0.0274	0.2488	0.0071	0.0514	0.1962	0.1168
34	(Methyl 3-deethyl-3-(1,3-oxazol-5-yl)-phytochlorinato)zinc(II) [catena-μ-Zn-oxazolyl-*N* polymer]	Zn(II)	ZOKMAP	36e	0.3746	0.0215	-0.3348	-0.0432	-0.0853	-0.0703	-0.0519	0.1072	0.4459	0.0489	0.0496	-0.3119	0.0801	-0.0227	0.2885	-0.0946
35	(Methyl pyropheophorbidato a)nickel(II)	Ni(II)	HAHBAT	16	1.3693	0.0443	-0.0965	1.3349	0.1668	-0.1605	-0.0604	0.1624	0.3422	0.0455	-0.016	-0.1132	-0.0817	-0.0701	-0.2914	-0.0867
36	(Methyl 20-methyl-phytochlorinato)nickel(II)	Ni(II)	YOVYAJ	37	1.7901	0.0481	0.6005	1.632	0.134	-0.3224	-0.0935	0.2228	0.4558	0.0547	0.0176	-0.1197	-0.0885	-0.1278	-0.3914	-0.1257
37	(Methyl 3-deethyl-3-hydroxymethyl-phytochlorinato)cadmium(II) [catena-((□^{2}-bacteriochlorophyll)-cadmium) polymer]	Cd(II)	UMAZAJ	38a	0.2908	0.0294	-0.1604	0.1501	-0.178	-0.0564	-0.0032	0.0378	0.3925	0.0777	0.0879	-0.1191	-0.1215	0.055	-0.3194	-0.1108
38	(Methyl phytochlorinato)platinum(II)	Pt(II)	KILQAZ	38b	0.1283	0.0174	0.0257	-0.0831	-0.0847	0.0129	0.0089	-0.0384	0.192	0.0458	0.048	-0.1124	-0.0566	0.0055	0.091	-0.1022
Other phytochlorins																				
S1	Benzimidazolo(2,1-*n*)purpurin-18 13^1-imino-13^2-imide methyl ester	2H	FOXTUH	39	0.2985	0.0222	-0.1789	0.2057	-0.0064	-0.0152	0.0352	0.1151	0.4504	0.0349	-0.2186	-0.1607	0.0235	0.0895	0.3466	-0.0229
S2	Methyl 3^1,3^2-didehydro-13^1-deoxo-quinoxaline(2,3-n)phytochlorin	2H	FOXWIY	39	0.3826	0.0285	0.2192	0.2666	-0.0143	-0.0975	-0.0908	0.0966	0.5015	0.0515	0.2943	-0.2972	-0.0691	0.0327	0.2405	-0.1135
Bacteriochlorophyll (a or b) derivatives																				
39a	Methyl bacteriopheophorbide a	2H	WIKSEO	40a	0.2226	0.0251	-0.1174	0.0133	-0.1051	-0.121	0.0856	0.0509	0.6275	0.0557	0.3041	-0.4118	-0.0836	-0.0425	0.3376	-0.0944
39b	Methyl bacteriopheophorbide a•0.5C_6H_6	2H	BAVSUM01	40b	0.2682	0.0296	-0.1692	0.0078	-0.137	-0.1235	0.0829	0.0487	0.6124	0.0538	0.2974	-0.3842	-0.0849	-0.0562	0.3476	-0.0882
39c	Methyl bacteriopheophorbide a• C_6H_6	2H	BAVSUM	40c	0.2879	0.0439	-0.1771	0.0797	-0.0842	-0.1419	0.0632	0.1179	0.7003	0.0796	0.2592	-0.4177	-0.1047	-0.3452	0.3197	-0.1281
β-Substituted Chlorins																				
Free base chlorins																				
40	7-Hydro-8,8-dimethylporphyrin	2H	PACRES	42a	0.1888	0.0201	-0.0636	-0.0431	0.0405	0.1381	-0.0122	-0.0942	0.2989	0.0308	-0.0231	-0.1028	-0.0079	0.0707	0.2706	0.0015
41	3-Bromo-7-hydro-8,8-dimethylporphyrin	2H	PACRIW	42b	0.314	0.0148	-0.2142	0.0227	-0.1911	0.0783	0.0828	-0.0523	0.276	0.032	0.0019	-0.0475	0.0146	0.0888	0.2565	0.0057
42	2-Acetyl-5-bromo-7-hydro-8,8-dimethylporphyrin	2H	MUMGAD	42b	0.3225	0.0144	0.1609	0.27	-0.0103	-0.0374	-0.0557	0.0246	0.2952	0.0342	-0.0545	-0.027	0.0261	0.0844	0.2749	-0.0058
43	5,10-Dibromo-7,7-dimethyl-15-phenyl-8-hydroporphyrin	2H	TACTID	42c	0.7558	0.0199	-0.5614	0.482	-0.1093	0.0999	-0.0288	0.0321	0.4682	0.0342	0.3145	-0.1618	0.0094	-0.1384	0.273	0.0188
44	7,7-Dimethyl-8-oxoporphyrin	2H	PACROC	42a	0.298	0.0068	-0.1641	-0.1624	-0.1707	0.0762	0.0123	-0.0194	0.2704	0.0295	0.0434	-0.0283	0.0128	0.0659	0.2555	0.0245
45	3,7,8,12,13,17,18-Heptaethyl-3-hydroxy-2-oxochlorin	2H	WANDEX	42d	0.1654	0.0187	0.0944	0.0756	-0.0715	0.052	-0.0438	-0.0549	0.2894	0.0292	-0.0251	-0.0768	-0.0491	-0.0309	0.2704	0.0275
46	20-Chloro-3,3,7,8,12,13,17,18-octaethyl-2-oxochlorin	2H	WANDAT	42d	0.2168	0.0119	0.1296	-0.0182	-0.0011	-0.1492	-0.0676	-0.0551	0.5087	0.0347	-0.3514	-0.022	-0.1066	-0.061	0.3449	-0.0279
47	3,3,7,8,12,13,17,18-Octaethyl-2-oxochlorin unknown solvate (mol. 1 N1-N4)	2H	WANBOF	42e	0.2013	0.0072	0.0707	0.0954	0.0080	-0.1297	0.0971	0.0104	0.2973	0.0296	-0.0791	-0.0412	-0.0533	-0.0104	0.2777	0.0185
"	" (mol. 2 N5-N8)	2H	"	42e	0.2724	0.0123	0.1407	-0.1614	-0.0132	0.0237	-0.1636	0.0294	0.4093	0.0311	-0.0453	-0.2828	-0.0627	0.0166	0.2824	-0.0387
48	3,3,7,8,12,13,17,18-Octaethyl-2-(hydroxyimino)-chlorin•$CHCl_3$	2H	WANCAS	42e	0.3422	0.0091	-0.2236	0.1192	-0.0218	-0.0688	0.2172	0.0234	0.3311	0.0287	-0.0994	-0.0626	-0.0581	-0.0035	0.304	-0.0004
49	3,3,7,812,13,17,18-Octaethyl-2-oxo-20-formyloxychlorin •$CHCl_3$	2H	WANCEW	42f	0.4135	0.0119	-0.2883	-0.1866	-0.1624	-0.0604	0.151	0.0164	0.3519	0.0321	-0.1553	-0.0298	-0.088	-0.036	0.2985	-0.0256
50	*cis*-2,3-Dihydroxy-2',3',7,8,12,13,17,18-octaethylporphyrin ethyl acetate solvate	2H	KOCZUX	42g	0.8136	0.0531	0.0324	0.7457	-0.1017	-0.1269	0.1866	-0.2087	0.234	0.0298	-0.0927	-0.0032	-0.0266	-0.0255	0.2117	-0.0023
51	Phyllochlorin ester	2H	PHLLCL10	42h	0.7863	0.0256	0.6967	0.2761	0.0894	0.1697	0.072	0.1209	0.2995	0.0372	0.1972	-0.0855	-0.0047	-0.0656	0.1965	0.0236
52	2,3-Bis(dicyanomethyl)-12,13-dibromo-5,10,15,20-tetraphenylchlorin chloroform methanol solvate	2H	NOCGER	42i	0.3656	0.032	0.0796	-0.2512	-0.0081	0.0213	-0.2456	0.0584	0.4137	0.0259	0.016	0.2553	0.0001	0.0007	0.325	0.012
53	*trans*-2,3-Di-n-butyl-5,10,15,20-tetraphenylchlorin dichloromethane solvate	2H	QAKLUJ	42j	0.4811	0.0415	0.2207	0.2682	-0.1649	-0.0506	0.2465	-0.1425	0.3085	0.0319	0.0008	0.1191	-0.0468	-0.0124	0.2803	-0.0096
54	12-Nitro-5,10,15,20-tetraphenyl-2,3-dihydroporphyrin-2,3-diol ethanol solvate hydrate	2H	TIPBIF	42k	1.9416	0.0261	1.9229	0.1931	-0.0395	0.0707	0.1678	-0.0149	0.199	0.0459	-0.0004	0.1817	-0.0648	-0.0087	0.0479	-0.0025
Metallochlorins																				
S3	(2,2-Dimethylchlorinato)zinc(II)•C_6H_6	Zn(II)	NIDFEM	43a	0.2957	0.0265	0.0816	-0.0455	-0.2136	0.0588	-0.1591	-0.0656	0.263	0.0292	-0.0293	-0.1655	-0.0485	0.0731	0.1822	-0.0015
S4	(12-Bromo-3,3-dimethyl-15-(4-methylphenyl)chlorinato)zinc(II)•$CHCl_3$	Zn(II)	XIPLEO	43b	0.6479	0.0511	0.5297	0.1002	0.3152	0.0791	0.0752	0.1337	0.213	0.0279	0.0562	-0.0891	0.0055	0.0456	0.179	-0.0103
S5	catena[(μ_2-2,2-Dimethyl-3-oxochlorinato)]zinc(II)•C_6H_6 / catena[(μ_2-Zn…O] polymer	Zn(II)	NIDFAI	43a	0.3438	0.0206	-0.226	-0.2061	0.0351	0.115	-0.0688	0.0739	0.2344	0.0233	0.0094	0.065	-0.0632	-0.0244	0.2114	0.0366
S6-1	Nitrosyl(2,2,7,8,12,13,17,18-octaethyl-3-oxochlorinato)iron(II)•$CHCl_3$	Fe(II)	QUJZUQ	43c	0.3041	0.0079	0.2311	-0.1924	0.0227	-0.0105	-0.0168	-0.0338	0.0814	0.018	0.0158	0.023	-0.0593	-0.003	0.0439	0.0202
S6-2	Chloro-(3,3,7,8,12,13,17,18-octaethyl-2-oxo-2,3-chlorinato)-iron(III)•$CHCl_3$	Fe(III)	LAMDUZ	43e	0.5769	0.0087	-0.5632	0.0603	-0.0165	0.1082	0.0068	0	0.1207	0.0253	0.0191	0.0815	-0.0518	0.0054	0.0688	0.0108
S7a^{i}	(3,3,7,8,12,13,17,18-Octaethyl-3H-porphin-2-onato)-nickel(ii) (mol. 1: N1-N4)	Ni(II)	DOZVIX01	43d	1.023	0.0109	-0.0003	1.0217	-0.0002	0.0002	0.0506	-0.0345	0.2343	0.031	0.0001	0.0267	-0.0211	-0.0002	-0.2318	0.0001
S7a^{ii}	" mol. 2: N5-N8	Ni(II)	"	"	0.4698	0.0091	0.4491	-0.1061	0.0231	-0.0839	0.0104	0.004	0.1336	0.027	0.0056	0.0227	-0.0584	-0.0249	-0.1139	0.0175
S7b	(3,3,7,8,12,13,17,18-octaethyl-2-oxochlorinato)nickel(II)	Ni(II)	DOZVIX02	42e	0.4396	0.0062	-0.0409	0.1244	-0.0075	0.0983	-0.0275	0.003	0.098	0.0207	-0.0098	0.0347	-0.0664	-0.0351	-0.0449	0.0253
S7c^{i}	(3,3,7,8,12,13,17,18-Octaethyl-2(3H)-chlorinato)nickel(II) (mol. 1:N1-N4)	Ni(II)	DOZVIX	43f	1.0338	0.0147	-0.0001	1.0318	0.0005	-0.0002	0.0411	-0.0508	0.144	0.0471	-0.0001	0.1196	-0.0297	0.0004	-0.0746	-0.0001
S7c^{ii}	" mol. 2: N4-N7	Ni(II)	"	"	0.4709	0.0085	0.4467	-0.1105	0.0374	-0.0779	0.043	-0.0256	0.1171	0.0302	-0.0376	0.0458	-0.0742	-0.0069	-0.0635	0.025
S8	(3,3,7,8,12,13,17,18-octaethyl-2-(hydroxyimino)chlorinato)-nickel(II) n-hexane n-pentane solvate	Ni(II)	WANBIZ	42e	0.2675	0.0135	-0.0247	-0.2184	-0.0222	0.1259	0.082	0.014	0.0708	0.0211	0.0254	0.0146	-0.0565	-0.0095	-0.0289	-0.0053
S9	7,13,17-Triethyl-2,8,12,18-tetramethyl-2-methoxycarbonylmethyl-3-methoxycarbonylmethylenechlorin-nickel(II) methanol solvate	Ni(II)	JUNZUN	43g	0.2799	0.0055	-0.2345	0.1472	0.0331	-0.0055	0.003	-0.0227	0.1375	0.0298	-0.0183	0.0347	-0.0617	0.0693	-0.0934	0.0042
S10^{i}	*rac*-(2,7,12,18-Tetramethyl-2,13,17-tris(2-methoxycarbonyl-	Ni(II)	PASXEM	44a	0.7608	0.0545	-0.0802	-0.6997	0.1727	-0.1622	0.0829	0.1407	0.1999	0.0334	0.0089	0.0467	0.0619	0.0073	-0.1825	0.0219

	ethyl)-3-oxo-porphinato)nickel(II) (mol. 1:N1-N4).																			
S10[ii]	" mol. 2: N5-N8.	Ni(II)	"	"	0.4171	0.0409	0.0277	0.1784	-0.1903	0.2124	-0.1071	-0.2204	0.1592	0.0428	-0.0398	-0.0115	0.0045	0.0148	-0.1503	0.0286
S11	(20-Ethoxycarbonyl-2,7,8,12,13,17,18-heptamethyl-3-methylidene-2-(p-tolylmethyl)-2-chlorinato)copper(II)	Cu(II)	NIJBOX	44b	0.4102	0.0278	-0.2317	0.3028	0.0045	-0.0887	0.0347	-0.1174	0.1849	0.0216	-0.088	0.055	-0.0887	-0.0566	0.1105	0.012
S12	(20-Ethoxycarbonyl-3,7,8,12,13,17,18-heptamethyl-2-methylidene-3-(p-tolylmethyl)-3-hydrochlorinato)copper(II)	Cu(II)	NIJBUD	44b	0.757	0.0352	0.6119	0.33	-0.0858	-0.0577	0.2078	-0.189	0.1078	0.0249	-0.0387	0.0057	-0.0422	-0.054	0.0713	-0.0178
S13	(20-Ethoxycarbonyl-2-(2-methoxycarbonylmethyl)-2,3,7,8,12,13,17,18-octamethyl-trans-chlorinato)copper(II)	Cu(II)	LICSEV	44c	0.7776	0.0538	-0.0461	-0.7288	0.1	0.0783	-0.149	0.1819	0.1419	0.0212	-0.0675	0.0358	-0.0839	-0.0624	0.0581	-0.0019
S14	(*trans*-2,3,7,8,12,13,17,18-Octaethyl-5,10-diformyloctachlorinato)copper(II)	Cu(II)	LOGYAH	44d	1.5201	0.0406	-0.6415	-1.2606	-0.0017	-0.0051	-0.5174	0.2058	0.0973	0.031	0.0306	0.0586	0.0282	0.0291	-0.0587	0.0018
S15	(2,2'-(5,10,15,20-tetraphenyl-2,3-chlorinato-2,3-diyl)bis(3-oxo-3-phenylpropanenitrile))nickel(II)	Ni(II)	XANDOI	44e	1.5781	0.0333	0.1019	1.559	0.0121	-0.0683	0.1249	-0.1702	0.3245	0.029	-0.0106	0.0562	-0.0287	-0.0557	-0.3131	-0.0087
S16	(2,3-Dimethyl-5,10,15,20-tetraphenyl-2,3-dihydroxy-2,3-chlorinato)nickel(II)	Ni(II)	ZAZNOF	44f	2.0996	0.0578	-0.1487	-2.0549	0.0414	-0.124	-0.325	0.2026	0.5012	0.0553	0.0318	0.0043	0.0866	0.0631	-0.4884	0.0111
S17	(2,3-bis(Dicyanomethyl)-7,8,12,13,17,18-hexabromo-5,10,15,20-tetraphenylchlorinato)nickel(II)•$CHCl_3$	Ni(II)	NOCGAN	42i	3.1927	0.0482	2.3319	-2.1384	-0.0149	0.1744	-0.3609	0.1482	0.8793	0.0997	-0.0236	-0.0335	0.1418	-0.1662	-0.8505	0.0216
Fused chlorins																				
S18	2,3,7,8,12,13,16,16-Octaethylbenzochlorin	2H	JUNZIB	43g	0.2678	0.014	-0.2177	-0.1132	0.0301	-0.0351	-0.0906	-0.0337	0.4907	0.0361	-0.3612	-0.1298	-0.0778	-0.01	0.2903	-0.0556
S19	Ethyl benzochlorin-27-acetate	2H	QIRHEE	45a	0.2339	0.0073	0.1786	-0.1112	-0.0123	0.099	-0.0165	0.015	0.4171	0.039	-0.2577	0.0808	-0.0301	-0.0898	0.2995	0.0494
S20	2,2,7,8,12,13,17,18-Octaethyl-benzo(3,4,5)porphyrinato-nickel(II)	Ni(II)	OEBPNI	45b	1.5918	0.0236	1.0997	1.1167	0.1451	-0.0037	-0.2375	0.0025	0.3068	0.0279	-0.0734	0.0185	-0.0019	-0.0187	-0.2929	-0.0474
S21	(20-(2-Formylvinyl)-2,3,7,8,12,13,17,17-octaethylbenzochlorinato)nickel(II)	Ni(II)	VUFTEV	45c	2.1843	0.0176	0.0483	-2.1514	0.1397	0.3335	-0.0906	0.0349	0.5312	0.0611	0.0409	0.0176	0.0146	-0.025	-0.5263	0.0491
S22	7-Amido-2,3,7,12,13,17,18,10^3-octaethylbenzochlorin	2H	XIXVAB	45d	0.2517	0.0164	-0.1455	0.1417	0.0198	0.0652	0.1247	-0.0438	0.3995	0.0377	-0.3263	-0.1099	-0.0789	-0.0298	0.1747	-0.0588
S23	(7-Cyano-2,3,7,8,12,13,17,18-octaethyl-10^3-oxobenzochlorinato)nickel(II)	Ni(II)	XIXTUT	45d	1.6953	0.0523	-1.3937	-0.8006	0.1093	0.0563	-0.4152	0.3212	0.3725	0.0312	0.0051	-0.0303	0.034	0.0261	-0.3626	-0.0671
S24	Anhydrobonellin methyl ester	2H	AHBONM	45e	0.708	0.0404	-0.4204	-0.4339	0.2605	-0.0977	0.2138	0.116	0.3367	0.0364	0.1914	-0.0997	0.0501	-0.0545	0.2458	0.0297
S25	5-(Benzylimino)-10-mesityl-22,22-dimethyl-4-oxa-8,24,25,26-tetra-azahexacyclo[19.2.1.16,9.111,14.116,19.02,7]heptacosa-1,6,9(27),10,12,14(26),15,17,19,21(24)-decaen-3-one cyclohexane solvate	2H	OJOXIV	45f	0.5474	0.0217	-0.2392	0.4774	0.0979	-0.0207	0.0118	-0.0656	0.3467	0.0381	0.0562	0.2396	0.0875	-0.009	0.2272	-0.0178
S26	(10-Mesityl-22,22-dimethyl-5-(phenylimino)-4-oxa-8,24,25,26-tetraazahexacyclo[19.2.1.16,9.111,14.116,19.02,7]heptacosa-1,6,9(27),10,12,14(26),15,17,19,21(24)-decaen-3-one)-(tetrahydrofuran)zinc(II)	Zn(II)	OJOXUH	45f	0.8982	0.0402	0.7512	0.4524	0.1471	0.0468	-0.0314	0.1144	0.2942	0.0293	-0.0056	-0.2139	0.0158	0.0771	0.1826	-0.0348
S27	10-Mesityl-22,22-dimethyl-5-(phenylimino)-4-oxa-8,24,25,26-tetra-azahexacyclo[19.2.1.16,9.111,14.116,19.02,7]heptacosa-1,6,9(27),10,12,14(26),15,17,19,21(24)-decaen-3-one	2H	OJOXOB	45f	0.5192	0.0189	0.1458	-0.4751	-0.0543	0.0062	0.129	-0.0551	0.3135	0.0363	-0.0193	-0.1861	0.0068	0.0925	0.2326	-0.0236
S28	*trans*-(13,17-bis(Methoxycarbonylethyl)-2,7,12,18-tetramethyl-8-vinyl-2,3-(4',5'-bis(methoxycarbonyl)benzo))chlorin	2H	PIRCOI	45g	0.4062	0.0192	0.3201	0.1443	-0.1267	-0.118	-0.0399	0.1008	0.2796	0.0279	0.0605	-0.0037	-0.0637	-0.0151	0.265	-0.0029
S29	*cis*-(13,17-bis(Methoxycarbonylethyl)-2,7,12,18-tetramethyl-8-vinyl-2,3-(4',5'-bis(methoxycarbonyl)benzo))chlorin	2H	PIRCIC	45g	0.7604	0.022	0.1296	-0.73	-0.1009	-0.0122	-0.0958	0.095	0.2487	0.0291	0.0256	0.0618	-0.0516	-0.0116	0.2333	-0.0121
S30[i]	$2^1,2^2$(N,N-Dicarbonyl-N-phenyl)-8,12-bis(2-(methoxycarbonyl)ethyl)-2,7,13,17-tetramethyl-18-vinyl-$2,2^1,2^2,2^3$-tetrahydrobenzo[b]porphyrin (mol. 1: N1-N4)	2H	NEZLOV	46a	0.4621	0.0104	-0.4491	-0.0022	-0.0083	-0.0094	-0.0984	0.044	0.3007	0.0326	-0.0272	-0.0254	-0.0199	-0.0636	0.2909	0.0013
S30[ii]	" mol. 2: N5-N8	2H	"	"	0.3404	0.0159	0.2786	-0.1355	0.0542	-0.0284	0.0719	-0.1049	0.3611	0.0349	-0.02	-0.0555	0.004	-0.0524	0.3521	0.0143
S31[i]	(14,19,24-Triphenyl-9,12,28,29,30-pentaazaheptacyclo[23.2.1.1^{10,13}.1^{15,18}. 1^{20,23}.0^{2,11}.0^{3,8}]hentriaconta-1(27),2(11),3(8),4,6,9,14,16,18,20(29),21,23,25-tridecaen-31-one 9-oxide)-nickel(ii) dichloromethane n-pentane solvate (mol. 1: N1-N4)	Ni(II)	XUCBEE	46b	1.5765	0.0153	0.1202	-1.5508	-0.1771	-0.0453	-0.1804	0.0112	0.3828	0.0308	-0.0327	0.0026	0.015	0.0208	-0.379	-0.0341
S31[ii]	" mol. 2: N5-N8	Ni(II)	"	"	2.0643	0.017	-0.6701	-1.9294	-0.2183	-0.1064	-0.175	-0.0077	0.5383	0.048	-0.0447	0.0089	0.0343	0.0762	-0.5293	-0.0223
S32	3,9,13-Tris(2-(Methoxycarbonyl)ethyl)-4,8,14,21-tetramethyl-26,28,29,30-tetra-azaheptacyclo(14.8.3.1^{2,5}.1^{7,10}.1^{12,15}.0^{20,27}.0^{21,25})triaconta-1,3,5,7(29),8,10,12,14,16,18,20(27),25-dodecaen-24-one	2H	YAQXET	46c	0.5937	0.0248	-0.2987	0.3863	0.1885	0.0669	0.2369	-0.1339	0.4592	0.0441	0.104	-0.2585	-0.0711	-0.0173	0.3569	0.0233
S33[i]	4,5,6,7-Tetrafluoro-10-(methylsulfanyl)-14,19,24-tris(pentafluorophenyl)-9-oxa-12,28,29,30-tetraazaheptacyclo[23.2.1.1^{10,13}.1^{15,18}.1^{20,23}.0^{2,11}.0^{3,8}]hentriaconta-1(27),2(11),3,5,7,12,14,16,18,20(29),21,23,25-tridecaen-31-one dichloromethane methanethiol solvate (mol.1: N1-N4)	2H	YACGOB	46d	0.6643	0.0359	0.0801	-0.4845	-0.1144	-0.1083	-0.4015	0.1187	0.2133	0.0266	-0.029	-0.0844	0.0061	0.0321	0.1876	-0.0356
S33[ii]	" mol. 2: N5-N8.	2H	"	"	1.167	0.0322	-0.0962	-1.027	-0.2243	-0.3177	-0.3594	0.1329	0.147	0.0339	-0.0194	-0.0638	0.0425	0.0677	0.1011	-0.0233
Bacteriochlorins																				
Free base bacteriochlorins																				
55	2,2,12,12-Tetramethylbacteriochlorin	2H	BENROD	48a	0.157	0.0124	0	-0.0001	-0.0001	0.1463	0.0569	-0.0001	0.4065	0.0685	-0.0703	-0.1957	0.0001	0.0001	0.3473	-0.0368
56	3,13-Dimesityl-8,8,18,18-tetramethylbacteriochlorin	2H	BENRIX	48a	0.796	0.178	0	0.684	-0.024	0.098	-0.394	0	1.103	0.693	0.719	-0.248	-0.084	0.547	-0.15	-0.556
57	2,12-Diethoxycarbonyl-5,15-diethyl-8,8,18,18-tetramethylbacteriochlorin	2H	ECASUZ	48b	0.0644	0.019	0.0001	-0.0006	-0.0003	-0.0612	-0.0203	0	0.575	0.0394	-0.3552	-0.2016	0.0005	-0.0001	0.4046	-0.0138
58	2,12-Diethoxycarbonyl-8,8,18,18-tetramethyl-5,15-bis(4-methylphenyl)bacteriochlorin	2H	ECAFUM	48b	0.276	0.044	0.0002	-0.0001	-0.0002	0.2031	-0.1869	0.0004	0.5655	0.0383	-0.223	-0.2764	-0.0001	0.0004	0.4397	-0.0187
59	3,13-Dimethylene-2,2',7,8,12,12',17,18-octaethylporphyrin hexane dichloromethane solvate	2H	CONHIW	48c	0.143	0.0155	0	0.0001	0.0001	0.0046	0.143	0.0001	0.4056	0.0341	-0.0821	0.1573	0.0001	-0.0002	0.3645	-0.0102
60	3,8,13,18-Tetrakis(Methoxycarbonylethyl)-2,8,12,18-tetramethyl-7,17-dioxobacteriochlorin	2H	RIPMAE	48d	0.2838	0.0129	0	0	0	0.1384	0.2478	0	0.3694	0.0408	0.0031	0.1762	0	0	0.32	-0.0546
61	Methyl 4-((12-(2,4-diphenylbut-1-en-3-yn-1-yl)-10-methoxy-7,7,17,17-tetramethylbacteriochlorin-2-yl)ethynyl)benzoate cyclohexane solvate	2H	SUVBES	48e	0.6208	0.0347	0.3952	-0.4592	-0.0254	-0.0303	0.0031	-0.1295	0.4212	0.0418	0.1622	-0.1575	0.034	-0.0024	0.3524	-0.0311
62	3,13-Bis(ethoxycarbonyl)-2,12-diethyl-[2,3-dihydro[1,4]dioxepino[5,6.7-ef]]-8,8,18,18-tetramethylbacteriochlorin	2H	UYITIH	48f	0.2918	0.0242	-0.2021	0.0502	-0.0755	-0.1176	-0.1068	0.1042	0.4297	0.0394	0.1237	-0.1627	0.0133	-0.0036	0.3776	0.0106
63[i]	5,10,15,20-Tetrakis(pentafluorophenyl)bis(2-benzyl-1,2-oxazolidine-4,5-diyl)[b,l]porphyrin (mol. 1: N1-N4)	2H	BAGKIG	48g	0.1251	0.021	0.0002	-0.0003	-0.0003	0.1072	-0.0645	-0.0004	0.2991	0.0261	0.0366	-0.0936	-0.0001	-0.0002	0.2815	-0.0112
63[ii]	" mol. 2: N5-N8	2H	"	"	0.0829	0.0068	0.0003	0	-0.0001	-0.0128	0.0819	0.0002	0.2852	0.0297	-0.0838	-0.0635	-0.0004	0	0.264	-0.0247
Metallated bacteriochlorins																				
S34[i]	(8,8,18,18-Tetramethyl-2,12-bis(*p*-tolyl)bacteriochlorin)-copper(II) (mol. 1: N1-N4)	Cu(II)	BENRET	48a	0.8966	0.0472	0.0967	0.8104	0.2321	-0.1134	-0.1192	0.2384	0.1745	0.0262	-0.0224	-0.1594	-0.0468	-0.0299	0.0372	-0.0073
S34[ii]	" mol. 2: N5-N8		"	"	0.8785	0.0426	0.6832	0.4554	0.0804	-0.1106	-0.0824	0.2685	0.157	0.0233	-0.0141	-0.1391	-0.0078	-0.0193	0.0631	-0.026
S34[iii]	" mol. 3: N9-N12		"	"	0.919	0.0557	0.364	-0.752	-0.1084	-0.1865	-0.1571	-0.2743	0.1598	0.0284	0.0391	-0.132	0.0077	0.0521	0.0614	0.0061
S34[iv]	" mol. 4: N12-N16		"	"	0.2784	0.0463	-0.0001	0	-0.0001	0.2702	-0.0671	0	0.2177	0.0369	-0.0303	-0.1808	0.0004	0.0002	0.1103	-0.0401

S35	ccc-Bacteriochlorinato-nickel(II) benzene solvate	Ni(II)	DEGTAK	49	1.9686	0.0701	-0.2706	-1.9064	0.018	-0.0662	-0.0204	0.4036	0.3831	0.0542	-0.0211	0.0293	0.0133	0.028	-0.3792	-0.0269
Isobacteriochlorins																				
Free base isobacteriochlorins																				
64	2,7-Dioxo-3,3,8,8,12,13,17,18-octaethylporphyrin	2H	SUCMIM	50a	0.2042	0.0123	-0.0237	-0.1875	0.0498	-0.0074	0.0484	-0.0337	0.4605	0.0474	0.3449	0.0024	-0.009	-0.0446	0.3003	0.0295
65	2,2,8,8,12,13,17,18-Octamethyl-isobacteriochlorin	2H	BEYXEI	50b	0.219	0.014	-0.0144	-0.19	-0.0299	0.0147	0.0834	-0.0598	0.3841	0.0429	0.1153	0.0005	-0.0689	-0.0587	0.3551	-0.0002
66	Dimethyl-octaethyl-isobacteriochlorin	2H	BEJKEG	50c	0.9902	0.061	-0.2179	0.9089	0.063	0.2219	0.2298	0.0312	0.2235	0.0357	0.1043	0.0434	-0.0179	-0.0079	0.1919	-0.0039
67	(+-)-(2RS,7RS)-Dimethyl 2,3,7,8-tetrahydro-17-(3-methoxy-3-oxoprop-2-enyl)-13-(3-methoxy-3-oxopropyl)-2,7,12,18-tetramethyl-3,8-dioxo-21H,23H-porphin-2,7-diacetate chloroform solvate	2H	KOSKEI	50d	0.2287	0.016	-0.0415	-0.1965	0.0532	-0.0273	-0.0408	0.0821	0.4479	0.038	0.3164	-0.0435	0.0052	-0.0046	0.3093	-0.0542
68	13,17-bis(2-Methoxycarbonylethyl)-12,18-bis(methoxycarbonylmethyl)-2,2,8,8,20-pentamethylisobacteriochlorin	2H	LEVXAL	50e	1.205	0.0441	-0.1025	-1.1122	0.1735	-0.2244	-0.3393	0.0944	0.4712	0.0382	0.3459	0.1439	0.02	-0.0057	0.2845	-0.0189
Metallo-isobacteriochlorins																				
S36	(Dioxoisobacteriochlorinato)copper(II) dichloroethane solvate	Cu(II)	DOMKOF	51a	0.2548	0.0124	0.1201	0.153	-0.0779	-0.0452	0.1295	-0.0473	0.1632	0.0326	0.0196	-0.0143	-0.0605	-0.0583	0.13	-0.0458
S37	(3,3,8,8,12,13,17,18-Octaethyl-3H,8H-porphine-2,7-dionato)-nickel(II)	Ni(II)	PETHEB	43a	1.3099	0.0165	0.1516	-1.2983	0.0532	-0.0416	0.0507	-0.0136	0.2249	0.0326	-0.0029	0.0242	0.065	-0.0317	-0.2064	-0.0465
S38	(1,3,6,7-Tetramethyl-4,5-bis(2-(methoxycarbonyl)ethyl)-1,7-bis(methoxycarbonylmethyl)-2,8-dioxoporphinato)nickel(II) unknown solvate	Ni(II)	VARFUP	51b	1.1981	0.0211	-0.7694	-0.8988	-0.0311	0.1144	-0.1171	0.0882	0.1953	0.032	0.0127	-0.0179	-0.0347	-0.0817	-0.167	-0.0435
S39	(Dimethyl 3,3'-(7,12-bis(2-methoxy-2-oxoethyl)-3,7,12,17-tetramethyl-8-oxo-13-thioxo-7,8,12,13-isobacteriochlorin-2,18-diyl)dipropanoatato)nickel(II) chloroform solvate	Ni(II)	SOXWUZ	51c	0.2337	0.0162	-0.0961	-0.1752	0.0643	0.0073	0.0651	-0.0792	0.0858	0.0306	0.0136	-0.0137	-0.0464	-0.0493	-0.0361	-0.0333
S40	(dimethyl 3,3'-(2,17-bis(2-methoxy-2-oxoethyl)-2,7,13,17-tetramethyl-3,18-dithioxo-17,18-dihydro-2H,3H-porphine-8,12-diyl)dipropanoato)-nickel hydrate	Ni(II)	SOXWOT	51c	1.1733	0.0262	0.5524	-1.0206	0.0015	-0.1279	-0.0634	-0.0982	0.1411	0.0298	-0.0111	0.009	0.0485	-0.0319	-0.1258	-0.0224
S41	(Anhydromesorhodoisobacteriochlorinato methyl ester)nickel(II)	Ni(II)	KODHAM	51d	1.9863	0.072	-0.2794	-1.9146	0.0316	0.2968	0.3237	-0.0878	0.4435	0.0599	0.0049	0.0471	-0.0553	-0.081	-0.4298	0.009
Manipulation of phytochlorin skeleton																				
24	Methyl phytochlorin	2H	KOVXUO	34b	0.1937	0.02	0.0489	-0.1291	-0.1302	-0.014	-0.0089	-0.0353	0.4816	0.0541	0.2639	-0.2931	-0.0557	0.0388	0.2388	-0.1216
69	Methyl phytoporphyrin	2H	RIWNOA	34a	0.2111	0.0088	0.045	-0.1917	0.049	-0.0045	-0.0532	0.0229	0.4086	0.0453	0.0381	-0.3551	-0.0756	-0.0235	0.1486	-0.105
70	3,7,8,12,13,17,18-Heptaethyl-2^1,2^2-dihydrocyclopenta[*at*]porphyrin (disordered)	2H	WIPDIJ	52a	0.1202	0.0165	0.0002	-0.0483	0.0022	-0.11	0.0047	0.0006	0.6685	0.2811	0.454	-0.0115	0.2716	0.1653	0.3435	-0.1469
71	3^1,3^2-Didehydrorhodochlorin-15-acetic acid trimethyl ester	2H	ZUBBIH	52b	0.3303	0.0335	-0.1907	0.1583	-0.0421	-0.155	0.0145	0.1471	0.4949	0.0383	-0.3777	0.051	0.0406	0.0734	0.3038	0.0189
72	3^1,3^2-Didehydrorhodochlorin dimethyl ester•CH_2Cl_2	2H	KUHPIM	52c	0.3661	0.022	0.3065	0.0683	0.1304	-0.06	-0.084	0.0884	0.3045	0.0332	-0.0168	0.0094	0.0095	0.0917	0.2893	0.0126